

The polarization of the planet-hosting WASP-18 system

KIMBERLY BOTT,^{1,2,3} JEREMY BAILEY,^{4,5} DANIEL V. COTTON,^{4,5} LUCYNA KEDZIORA-CHUDCZER,^{4,5}
JONATHAN P. MARSHALL,⁶ AND VICTORIA S. MEADOWS^{1,2,3}

¹*University of Washington Astronomy Department
Box 351580, U.W.
Seattle, WA 98195 USA*

²*Virtual Planetary Laboratory
Box 351580, U.W.
Seattle, WA 98195 USA*

³*University of Washington Astrobiology Program
Box 351580, U.W.
Seattle, WA 98195 USA*

⁴*School of Physics, UNSW Sydney
Kensington, Sydney, NSW 2052, Australia*

⁵*Australian Centre for Astrobiology, UNSW Sydney
Kensington, Sydney, NSW 2052, Australia*

⁶*Academia Sinica, Institute of Astronomy and Astrophysics,
11F Astronomy-Mathematics Building, NTU/AS campus,
No. 1, Section 4, Roosevelt Rd., Taipei 10617, Taiwan*

(Received September 12, 2018; Revised October 12, 2018; Accepted November 16, 2018)

Submitted to AJ

ABSTRACT

We report observations of the linear polarization of the WASP-18 system, which harbors a very massive ($\sim 10 M_J$) planet orbiting very close to its star with an orbital period of 0.94 days. We find the WASP-18 system is polarized at ~ 200 parts-per-million (ppm), likely from the interstellar medium predominantly, with no strong evidence for phase dependent modulation from reflected light from the planet. We set an upper limit of 40 ppm (99% confidence level) on the amplitude of a reflected polarized light planetary signal. We compare the results with models for a number of processes that may produce polarized light in a planetary system to determine if we can rule out any phenomena with this limit. Models of reflected light from thick clouds can approach or exceed this limit, but such clouds are unlikely at the high temperature of the WASP-18b atmosphere. Additionally, we model the expected polarization resulting from the transit of the planet across the star and find this has an amplitude of ~ 1.6 ppm, which is well below our detection limits. We also model the polarization due to the tidal distortion of the star by the massive planet and find this is also too small to be measured currently.

Keywords: polarization – techniques: polarimetric – planets and satellites: atmospheres – planets and satellites: individual: WASP-18b

1. INTRODUCTION

Hot Jupiters are often thought to provide ideal cases to study polarization from exoplanet atmospheres. Since the amount of light being scattered off a planet’s atmosphere will increase with radius (scattering disk) and inversely with

the distance to the star (incident flux), for a given atmosphere a larger hot Jupiter orbiting more closely to its star should produce a better signal. Furthermore a hotter star will produce greater flux in blue wavelengths which are preferentially Rayleigh scattered, a polarizing effect. Seager et al. (2000) modelled the expected polarization levels for hot Jupiter-type systems and predicted that linear polarization varying over the orbital cycle at the tens of parts-per-million level might be present in the combined light of the star and planet. The star—particularly if an inactive FGK dwarf—is typically expected to not contribute much, if any of this polarized light (Kemp et al. 1987; Stam et al. 2004; Cotton et al. 2017a). Rayleigh scattering from small cloud particles is anticipated to be the dominant source of polarization for a hot Jupiter contributing to this signal (Seager et al. 2000; Bailey et al. 2018) and hence the observation of polarization would be a strong indicator of the presence of clouds; the presence of clouds increasing the albedo may also be important (Fauchez et al. 2017). Detection of polarized light from a hot Jupiter can confirm or provide the color of the planet (Berdyugina et al. 2011), the nature of its bulk atmospheric composition (e.g. strong or weak Rayleigh scatterers, high clouds, no clouds or haze (Seager et al. 2000; Stam et al. 2004; Fauchez et al. 2017)), and the orbital parameters (Fluri & Berdyugina 2010) even without imaging the planet.

Despite the advantages of using polarimetry to detect and characterize planets, no polarization signal from a hot Jupiter has been detected to date. Past attempts at polarized light detection such as those described in Lucas et al. (2009) have not detected significant planetary polarization signals and the initial report of polarized light from HD 189733b has not been independently confirmed (see: Berdyugina et al. 2011; Wiktorowicz et al. 2015; Bott et al. 2016). Modern polarimeters currently available such as HIPPI (Bailey et al. 2015) and POLISH2 (Wiktorowicz & Nofi 2015) are now capable of detecting polarization at the parts-per-million level, which should be sufficient for detecting Rayleigh scattering polarization signals from hot Jupiters (Seager et al. 2000; Hough & Lucas 2003). If the predicted polarized light signals from hot Jupiter exoplanets continue to be undetectable this would suggest either a fundamental misunderstanding of their atmospheres, or a problem with the methodology in observing them in polarized light.

An important step in making polarimetry a viable approach to exoplanet characterization is the consideration of the many environmental factors that can contribute to a polarized light signal (e.g. interstellar polarization, circumstellar matter, tidal distortion, stellar activity, transit polarimetry, etc.). The estimates of polarized light signals from Seager et al. (2000) are based on the Rayleigh scattering of an idealized atmosphere, but other processes from the atmosphere and environment can polarize light while some (like multiple scattering) can dampen the polarization. In the meantime, providing upper limits to a planet’s polarized light signal can rule out certain types of planetary phenomena, including clouds (Seager et al. 2000; Stam et al. 2004; Fauchez et al. 2017), if these secondary processes are well characterized.

Here we report observations of polarization from the WASP-18 (HD 11069) system, which harbors a very massive ($10 M_J$ (Southworth et al. 2009)) planet orbiting very close to its star ($P \approx 0.94$ days, Hellier et al. 2009).

The WASP-18 system may provide an even more promising candidate for polarimetry than the well-studied hot Jupiter HD 189733b which produced a non-detection in polarized light (Wiktorowicz et al. 2015; Bott et al. 2016) although it was seen as a promising candidate. Owing to hydrostatic equilibrium, WASP-18b’s radius is approximately the same ($R \approx 1.165 R_J$, Southworth et al. 2009) as less massive hot Jupiters, including HD 189733b ($R \approx 1.138 R_J$, Torres et al. 2008). However the proximity of the planet to the star means the planet receives much more light from the star than those hot Jupiters in longer period systems of the same stellar type. The host star is a late F type, producing more blue light than HD 189733 (an early K dwarf). In our analysis of the signal we take into consideration the effects of clouds and environmental phenomena which may reduce or complicate the signal.

2. OBSERVATIONS

The WASP-18 system was observed over four observing runs on the 3.9-m Anglo-Australian Telescope (AAT) at Siding Spring Observatory in Australia. The observations were made with the HIgh Precision Polarimetric Instrument (HIPPI, Bailey et al. 2015) in “clear” mode (i.e. no filter) to allow a maximum signal.

The dates of observations were August 28–September 2, 2014; June 27th, 2015; October 14th–October 20th, 2015; and November 30th–December 7th, 2016. Most of these observations have total integration times of 2560–3840 seconds. However, the October 2015 observations include several shorter integrations of 640 seconds during and around the planet’s transit. HIPPI is an aperture polarimeter using a ferroelectric liquid crystal (FLC) modulator, a Wollaston prism analyzer and two photomultiplier tubes (PMT) as detectors. The FLC provides a 500 Hz primary modulation which is used together with two additional stages of slower modulation obtained by rotation of the Wollaston prism and detectors, and finally by rotating the whole instrument to four position angles (0, 45, 90, 135 degrees) using the AAT’s Cassegrain rotator. As with our measurements of HD 189733b these redundant angles were measured to

account for instrumental polarization. The sky background signal is subtracted from the data using a sky observation made immediately after each science observation at each Cassegrain rotator position.

HIPPI achieves a precision of 4.3×10^{-6} (4.3 parts-per-million or ppm) or better on bright stars (Bailey et al. 2015). This is comparable to or better than the precisions reported from polarimeters based on photoelastic modulators such as the Pine Mountain Observatory polarimeter (Kemp & Barbour 1981), PlanetPOL (Hough et al. 2006), POLISH (Wiktorowicz & Matthews 2008) and POLISH2 (Wiktorowicz & Nofi 2015; Wiktorowicz et al. 2015). It is sensitive enough to detect polarized light from a Rayleigh scattering hot Jupiter atmosphere, expected to be on the order of parts- to tens-of-parts-per-million (Seager et al. 2000).

The detectors were Hamamatsu H10720-210 PMT modules that have ultra-bialkali photocathodes with a peak quantum efficiency of 43 per cent at 400 nm. The WASP-18 observations were made without a filter in an attempt to maximize the signal on this relatively faint object ($B = 9.7$). In this mode the wavelength response extends from 350 to 700 nm but is peaked towards the blue end of this range. Using our bandpass model (Bailey et al. 2015) we find an effective wavelength of 474 nm for the F6 spectral type of WASP-18.

The telescope introduces a small polarization (telescope polarization or TP) that must be corrected for. As described in Bailey et al. (2015) we determine the TP using observations of a number of stars we believe to have very low polarization either based on previous PlanetPol observations (Hough et al. 2006; Bailey et al. 2010) or because of their small distances and expected low levels of interstellar polarization (see Bailey et al. 2010; Cotton et al. 2016) listed in Table 1. The telescope polarization has been found to be stable during each run, but changes each time the telescope mirror is re-aluminized, which is done every year for the AAT. Analysis of our WASP-18 data averaged over each run shows no evidence for any changes between run that might be attributed to the TP calibration, and the standard deviation is the same for Stokes Q and U.

Full details of the observation, calibration, and data reduction procedures with HIPPI can be found in Bailey et al. (2015).

3. RESULTS

Table 2 lists the individual polarization observations of WASP-18, corrected for telescope polarization using the values in Table 1. We list the mid-point time, and the normalized Stokes parameters Q/I and U/I given in parts-per-million (ppm) on the equatorial system. The measurements are corrected for the wavelength dependent modulation efficiency of the instrument. This is calculated using the bandpass model described by Bailey et al. (2015). The value is close to 81.3 per cent for all of these observations.

Orbital phase is calculated according to the ephemeris where zero phase corresponds to mid-transit. Our adopted epoch is from Maxted et al. (2013), the period is from Wilkins et al. (2017).

$$T = \text{HMJD } 2455265.5525 + 0.94145287 \text{ E.} \quad (1)$$

Typically we observed WASP-18 a few times per night; the average error of each of these unbinned data points is 33.3 ppm. This is on par with *nightly mean* errors from other polarimeters on hot Jupiter systems (e.g. Wiktorowicz et al. (2015)).

Two important observations can be made from the data: first, there is clear evidence of polarization at a level of ~ 200 ppm, and second that the unbinned data points are in reasonable agreement with each other. The latter point suggests that our instrument is reliable, and that there is little contribution from noise sources over short time scales (such as star spots).

In fitting simple Rayleigh curves to the data, there is no significant difference between using the individual transit points and binned points (by phase). The data points within transit are inherently noisier due to the shorter duration of the observations, but their inclusion does not significantly change the best fit for the Rayleigh curve. Although the polarization values vary by over 200 ppm, the best fit curve of the polarization ($P = \sqrt{Q^2 + U^2}$) has an amplitude of 16.9 ± 9.8 ppm. This 200 ppm variation may be entirely from noise imparted by the many processes that contribute to the polarization, although we show that some portion of the variation may be from a modulated signal in Section 3.2. Even in the best circumstances hot Jupiters are not expected to produce signals stronger than a few tens of parts-per-million, thus this fit would be in the realm of a reasonable detection if it were shown to be from the planet in the future as more polarimetric measurements of the system, or observation on a larger telescope, would drive down the noise.

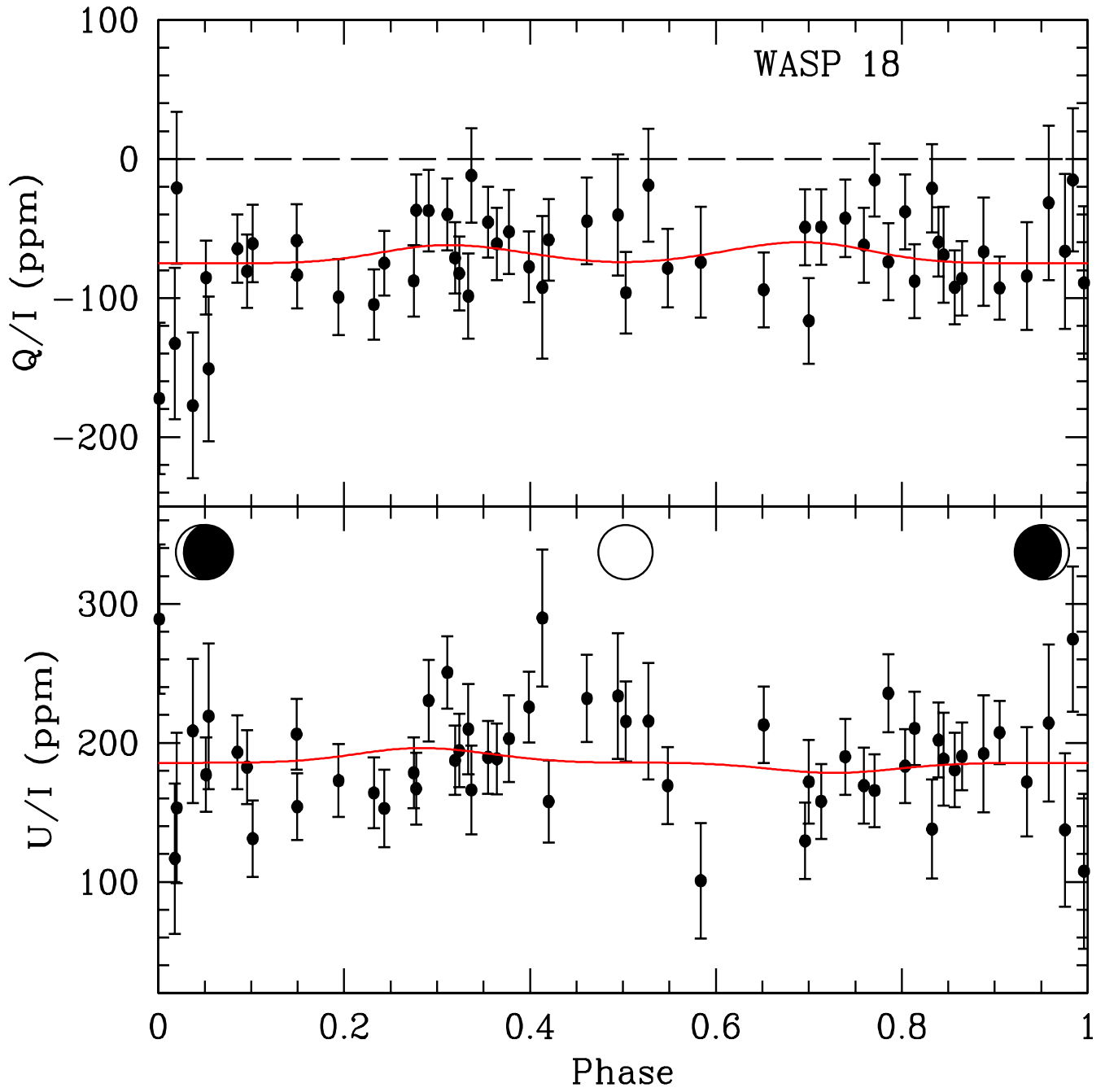


Figure 1. HIPPI measurements of the polarized light from the WASP-18 system including those taken over the transit and secondary eclipse. The data are not binned by run nor by phase. The red curve is a least squares fit of a Rayleigh-Lambert model as described in Section 3.1. This represents a simplified case where the system polarization would be dominated by Rayleigh scattering in the planet’s atmosphere alone. Note the change in the y-axis for Stokes Q and U.

Table 1. Low polarization star measurements to determine telescope polarization (TP) in the “Clear” setting (no filter) for the four observing runs referred to in this paper. Theta, θ , refers to the position angle.

Star	Date	Q/I	U/I	p (ppm)	θ ($^\circ$)
HD 2151	29 Aug	30.0 ± 3.1	-41.8 ± 3.1		
HD 2151	31 Aug	34.2 ± 3.1	-47.8 ± 2.9		
Adopted TP	Aug 2014	32.1 ± 2.2	-44.8 ± 2.1	55.1	117.2
HD 48915	23 May	-35.0 ± 0.8	-3.2 ± 0.8		
HD 140573	22 May	-39.2 ± 3.5	3.1 ± 3.4		
HD 140573	25 May	-47.5 ± 9.7	-17.4 ± 11.0		
HD 140573	27 Jun	-38.6 ± 2.9	3.7 ± 3.0		
Adopted TP	May 2015	-40.1 ± 1.6	-3.5 ± 1.8	40.2	92.5
HD 2151	14 Oct	-61.9 ± 3.4	-4.9 ± 3.5		
HD 2151	15 Oct	-54.9 ± 3.2	-3.0 ± 3.2		
HD 2151	16 Oct	-56.0 ± 3.2	-6.9 ± 3.1		
HD 2151	17 Oct	-47.7 ± 3.9	3.5 ± 3.9		
HD 2151	19 Oct	-45.4 ± 3.3	2.8 ± 3.2		
HD 48915	14 Oct	-44.2 ± 1.1	-3.7 ± 0.9		
HD 48915	15 Oct	-43.8 ± 0.7	3.1 ± 0.7		
HD 48915	15 Oct	-51.0 ± 0.8	-1.1 ± 0.7		
HD 48915	16 Oct	-52.4 ± 0.6	-4.1 ± 0.6		
HD 48915	17 Oct	-48.6 ± 8.7	4.0 ± 11.3		
HD 48915	20 Oct	-46.9 ± 4.6	1.4 ± 3.2		
Adopted TP	Oct 2015	-50.1 ± 0.4	-0.8 ± 0.3	50.3	90.5
HD 2151	30 Nov	-33.9 ± 3.5	6.9 ± 3.4		
HD 48915	30 Nov	-23.3 ± 2.5	8.8 ± 2.7		
HD 48915	1 Dec	-20.6 ± 0.8	6.3 ± 0.8		
HD 48915	1 Dec	-17.2 ± 4.9	-21.0 ± 5.1		
HD 48915	2 Dec	-24.0 ± 1.3	1.2 ± 1.6		
Adopted TP	Dec 2016	-23.8 ± 0.4	0.4 ± 0.5	23.8	89.5

Our parameter values for the models throughout this section are taken from [Southworth et al. \(2009\)](#) which derived values for semi-major axis, a , planetary radius, R_p , and stellar radius, R_* comparing observational fits with different stellar models and compares these values to those in literature, finding they are largely in good agreement (with some discrepancy from the *Cambridge* stellar models). The radius of a transiting planet is always contingent upon the certainty of the stellar type and distance to the system, as it is a ratio of the radii (of star and planet) that are retrieved from the normalized reduction in the flux. Our $(R_p/a)^2$ —which is used to scale our direct beam (stellar source) and in the forward radiative transfer and simplified Rayleigh models—is 0.00074. A gravitational acceleration based on the mass is also used in our forward models for the atmospheric model used as input to the radiative transfer solution; here we also adopt the value from [Southworth et al. \(2009\)](#) of 191 m/s.

3.1. Rayleigh-Lambert model

Our data is fitted with a Rayleigh-Lambert model for the expected polarization variation. This is an analytic model which calculates the intensity according to the expected phase variations for a Lambert sphere, and assumes the polarization follows the phase function for Rayleigh scattering (see: [Seager et al. \(2000\)](#) and [Wiktorowicz \(2009\)](#)). To find the best fit we use a Levenberg-Marquardt non-linear least squares algorithm ([Press et al. 1992](#)) with five parameters: the polarization zero point offsets in Q/I and U/I (Z_q and Z_u), the polarization amplitude p which allows the effects of depolarization processes such as multiple scattering to be taken into account, the position angle of the major axis of the projected orbit ellipse on the sky PA , and the orbital inclination i . The fitted parameters and their

Table 2. The fully calibrated WASP-18 polarization observations without binning.

UT Date and Time	Q/I (ppm)	U/I (ppm)	UT Date and Time	Q/I (ppm)	U/I (ppm)
2014-08-28 16:02:41	-58.6 ± 26.1	206.4 ± 25.5	2015-10-16 16:16:59	-92.1 ± 22.7	207.7 ± 22.8
2014-08-28 17:04:03	-99.3 ± 27.2	172.9 ± 26.2	2015-10-17 10:14:36	-115.8 ± 30.8	172.4 ± 30.1
2014-08-28 18:10:35	-74.7 ± 23.2	152.9 ± 27.7	2015-10-17 13:14:14	-20.7 ± 31.8	138.1 ± 35.7
2014-08-29 16:31:05	-104.5 ± 25.3	164.1 ± 25.4	2015-10-19 10:35:11	-59.2 ± 24.9	202.2 ± 26.8
2014-08-29 17:32:44	-36.8 ± 25.7	167.0 ± 25.9	2015-10-19 13:51:05	-14.2 ± 51.4	274.7 ± 52.4
2014-08-29 18:35:31	-82.1 ± 26.5	194.5 ± 26.4	2015-10-19 14:14:18	-171.3 ± 54.4	289.6 ± 53.7
2014-08-30 16:04:47	-87.6 ± 25.7	178.6 ± 25.4	2015-10-19 14:39:50	-20.3 ± 54.6	153.2 ± 54.2
2014-08-30 17:05:02	-71.1 ± 25.7	187.5 ± 25.0	2015-10-19 15:03:15	-176.8 ± 52.4	209.2 ± 51.9
2014-08-30 18:05:58	-61.0 ± 25.9	188.5 ± 25.5	2015-10-19 15:26:07	-150.2 ± 52.0	219.7 ± 52.4
2014-08-31 15:29:42	-39.6 ± 25.9	250.7 ± 26.0	2015-10-19 16:08:19	-64.0 ± 24.6	193.4 ± 26.5
2014-08-31 16:28:50	-45.3 ± 25.4	189.6 ± 26.1	2015-10-20 11:19:37	-83.6 ± 38.7	172.2 ± 39.3
2014-08-31 17:28:44	-77.4 ± 25.6	225.9 ± 25.5	2015-10-20 11:51:32	-30.9 ± 55.7	214.4 ± 56.5
2014-09-02 17:01:17	-96.0 ± 29.4	215.5 ± 28.8	2015-10-20 12:15:20	-66.0 ± 55.8	137.7 ± 55.2
2014-09-02 18:02:16	-78.4 ± 28.3	169.3 ± 27.7	2015-10-20 12:43:01	-88.7 ± 55.0	107.9 ± 55.8
2014-09-02 18:50:29	-74.1 ± 39.9	100.8 ± 41.4	2015-10-20 13:12:52	-132.3 ± 54.5	117.3 ± 54.1
2015-06-27 17:27:43	-85.2 ± 26.5	177.2 ± 26.8	2015-10-20 15:06:19	-60.5 ± 27.9	131.3 ± 27.5
2015-06-27 18:27:26	-80.7 ± 26.3	182.7 ± 26.6	2015-10-20 16:11:16	-83.0 ± 23.8	154.4 ± 24.0
2015-10-14 13:21:30	-93.5 ± 27.0	213.2 ± 27.4	2016-11-30 13:26:59	-13.5 ± 33.9	160.5 ± 32.0
2015-10-14 14:21:53	-48.7 ± 27.3	129.7 ± 27.6	2016-12-01 11:00:29	-40.0 ± 29.4	224.2 ± 29.5
2015-10-14 15:20:17	-42.0 ± 27.8	190.1 ± 27.4	2016-12-01 11:58:27	-101.1 ± 30.7	202.4 ± 32.6
2015-10-14 16:23:14	-73.2 ± 27.7	236.0 ± 27.9	2016-12-01 12:57:55	-54.8 ± 30.3	196.6 ± 31.3
2015-10-15 13:20:53	-48.4 ± 27.0	158.1 ± 26.9	2016-12-01 13:55:28	-59.6 ± 29.5	151.2 ± 29.6
2015-10-15 14:23:17	-61.5 ± 26.9	169.4 ± 27.2	2016-12-01 14:51:31	-47.6 ± 31.2	225.6 ± 31.4
2015-10-15 15:23:31	-37.4 ± 26.9	183.5 ± 26.5	2016-12-03 10:58:08	-96.4 ± 51.3	282.5 ± 49.1
2015-10-15 16:46:18	-85.4 ± 26.7	190.6 ± 24.4	2016-12-04 11:24:03	-43.2 ± 43.5	227.6 ± 45.1
2015-10-16 13:14:56	-14.5 ± 26.3	165.7 ± 26.2	2016-12-04 12:08:31	-21.4 ± 40.6	209.9 ± 42.0
2015-10-16 14:13:00	-87.2 ± 26.6	210.7 ± 26.5	2016-12-07 15:06:22	-71.0 ± 34.5	181.6 ± 33.5
2015-10-16 15:11:33	-91.7 ± 26.7	180.8 ± 26.6	2016-12-07 16:04:50	-68.9 ± 38.9	185.5 ± 42.1

Table 3. Parameters of Rayleigh-Lambert fit to HIPPI linear polarization observations of WASP-18. Z_q and Z_u are the polarization offsets due to constant sources such as interstellar polarization, p refers to the strength of the polarized light modulation from Rayleigh scattering in the planet atmosphere, PA the position angle offset of the orbital plane, and i its inclination.

Parameter	Value	units
Z_q	-75.2 ± 6.0	ppm
Z_u	185.0 ± 5.5	ppm
p	16.2 ± 10.0	ppm
PA	200.3 ± 20.7	degrees
i	79.2 ± 10.9	degrees

uncertainties (determined from the covariance matrix of the fit) are listed in Table 3. The fitted model is shown by the red curve in Figure 1.

The best fit inclination for this system from our data ($79.2 \pm 10.9^\circ$) is lower than that suggested by the transit and phase curve model fitting done by [Hellier et al. \(2009\)](#) ($86.0 \pm 2.5^\circ$), though they overlap, and are hence consistent, within their errors. We can fit the Rayleigh-Lambert model with the inclination fixed at 86 degrees, and obtain very similar results, with $p = 17.3 \pm 10.2$ ppm. The impact parameter for this system reaches unity (a skimming transit) at an inclination of about 74 degrees. Thus the fitted model is consistent with the transiting nature of the system.

Table 4. Moment calculations: the terms are described in the text.

data	std dev	skewness	kurtosis
q	35.0	0.6320	4.1286
u	39.0	0.0847	3.4414

However, the error on the polarization amplitude is such that the fitted signal cannot be considered a significant detection of planetary polarization. Furthermore, when we account for statistical bias effects we will show that it is even less significant than it appears at first sight.

To improve our sensitivity to such effects we would need either substantially more data, or an instrument like HIPPI on a larger telescope. With an 8-meter class telescope we would be able to halve the uncertainties.

3.2. Statistical Tests

A simple way to check for variability in polarimetric data is to calculate the moments of the distribution for the Q and U data and compare the values with tables to determine significance. Table 4 presents our calculations of standard deviation, skewness and kurtosis for both Q and U; the skewness being the division of the 3rd moment of the data set squared by the second cubed, and the kurtosis being the 4th moment of the data set, divided by the second moment squared. The average uncertainty in our data is 33.3 ppm, a value that represents the internal standard deviation of individual measurements and which scales with photon-shot noise. The standard deviation (or scatter) in both Q and U is higher than 33.3 ppm, which may indicate some real variability. The scale of the additional variability may be calculated as $\sqrt{x^2 - e^2}$, where x is the scatter, and e the average error; for this data the values are 10.8 ppm in Q and 20.3 in U, the mean of which is similar to the fitted value of polarization, p in the Rayleigh model. The difference between the scatter and mean uncertainty could be due to a real signal, but it may also be accounted for by differences in centring, minor differences in telescope polarization (TP) calibration between runs or other systematics. As mentioned in section 2 there do not appear to be significant TP calibration difference between runs.

Using the significance tables given by Brooks et al. (1994) for $n = 56$, we see that in U both skewness and kurtosis are consistent with a Gaussian distribution. The fitted Rayleigh model amplitude is greater in Q than U though, and in Q we see some evidence for non-Gaussian behaviour. In Q the skewness is non-Gaussian at the 95% confidence level (0.6097 ± 0.0032), but not the 99% confidence level (0.8404 ± 0.0054). The kurtosis doesn't quite meet the threshold for being non-Gaussian at 95% confidence (4.2931 ± 0.0177), but it is high. In Q the skewness is positive, and the kurtosis high; together this implies a greater number of more positive outlying data points than expected from a normal distribution, and this is consistent with the form of the Rayleigh fit to the Q data shown in Figure 1.

When fitting a polarization amplitude to the observations as in the previous section it should be noted that the amplitude is subject to a statistical bias since the fitted amplitude can never be negative. The effect is analogous to the bias well known to be present in measurements of the degree of polarization (e.g. Simmons & Stewart 1985). The bias is most significant when the signal-to-noise ratio is small.

To test the size of this effect we carried out a set of trials where we generated random data sets with the same phasing and noise properties as our data, and fitted Rayleigh-Lambert models in the same way as just described. The results are shown in Figure 2. The black histogram represents a bootstrap sampling where we used the actual data points but randomly swapped them in phase. The red histogram represents data generated with a zero amplitude signal but noise randomly added in line with the errors of the actual data points. Both of these tests which were run for 10,000 trials generated very similar histograms, with a mean fitted amplitude of about 12 ppm. Of these trials 27% produced fitted amplitudes greater than the 16.2 ppm amplitude fitted to the actual data even though there was zero true signal in the generated data.

The green and blue histograms are for cases where the injected signal had amplitudes of 20 ppm and 40 ppm respectively. The 40 ppm injected signal produced fitted amplitudes higher than our 16.2 ppm signal, more than 99% of the time. Hence we can rule out a planetary signal of 40 ppm or greater at the 99% confidence level.

3.3. Constant polarization

A few different processes can lead to a polarized light signal outside of the modulated signal from the planet. In the cases of contributions from zodiacal dust and the interstellar medium (ISM) they are separable from the planetary signal in theory because they produce a constant signal, an offset in Stokes Q and U from zero, however these still contribute to the noise in the signal.

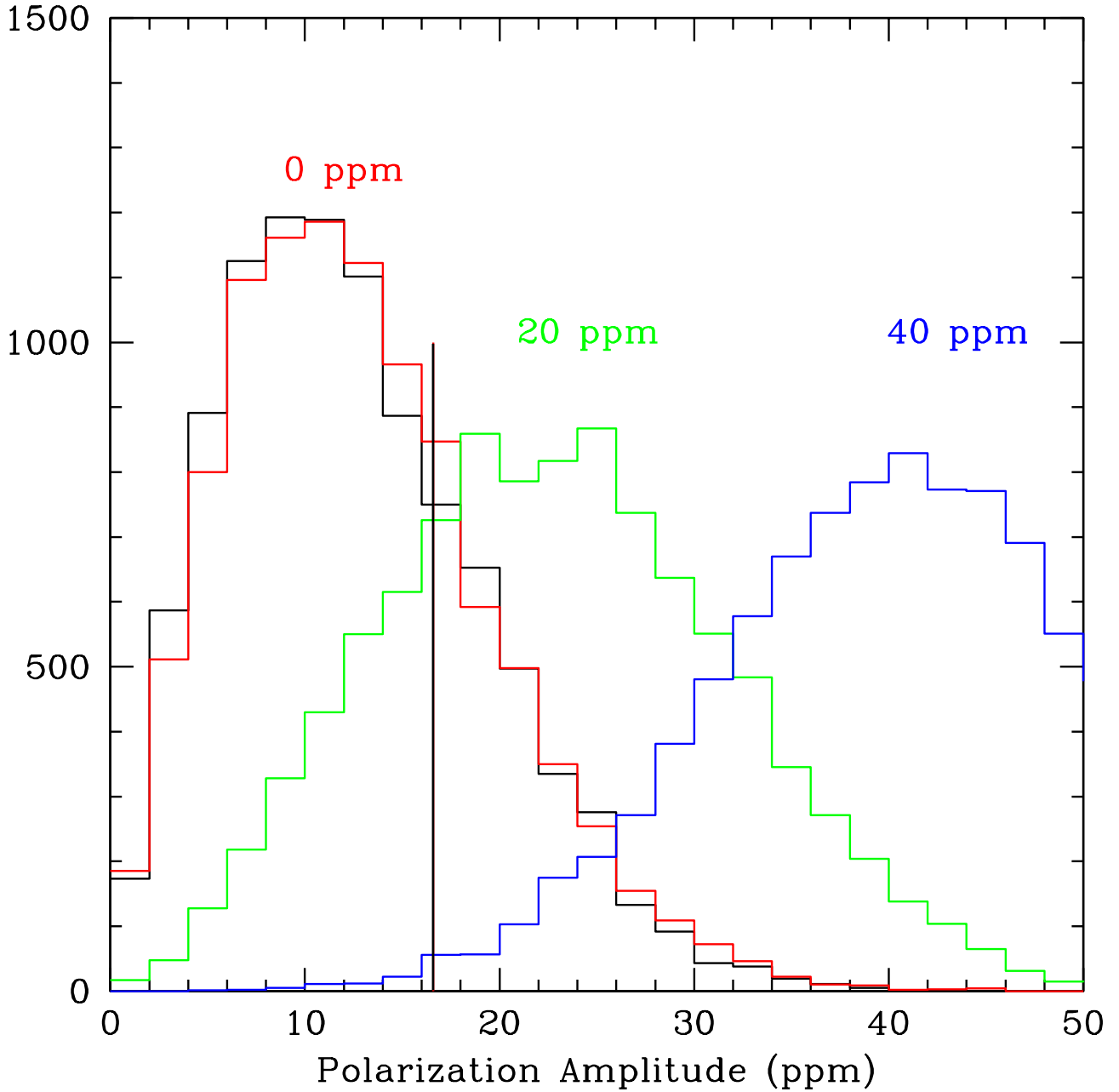


Figure 2. A confidence test with random sampling for detections at the 0 (red), 20 (green) and 40 (blue) ppm level. The black histogram corresponds to a bootstrap random sampling for 0 ppm. The 0 ppm samples are offset from a zero ppm amplitude because scattered data points may be fit to a zero amplitude curve when they do not coincide with a Rayleigh phase curve shape. Our observed polarization amplitude is shown by the vertical black line. This lies well into the wings of the 40 ppm curve where we can rule out a detection at the 40 ppm level with 99% confidence.

In our paper on HD 189733 (Bott et al. 2016), an offset in the modulated signal from zero was detected. This background polarization can be due in large part to interstellar polarization from the interstellar medium (Bailey et al. 2010; Cotton et al. 2016) and hence can be approximated if the polarization of the ISM is well characterized. WASP-18 is 126.4 parsecs from Sol (The Gaia Collaboration et al. 2016), at galactic coordinates 279.7100, -69.3214. Considering the trends in interstellar polarization from Cotton et al. (2016), we can estimate the expected offset from modulation

Table 5. Observations of control stars for WASP-18. Spectral type, distance, and position have been taken from SIMBAD. “Sep” is the angular separation from WASP-18.

Object	SpT	dist(pc)	Sep(deg)	Observed (UT)	Exp(s)	Q (ppm)	U (ppm)	p (ppm)	PA (deg)
HD 9414	A1V	99.6	1.0134	2015-10-16 17:53:47	640	-41.0±13.2	186.7±13.3	191.2±13.3	51.2±2.0
HD 9733	G8IV	122.0	0.5387	2015-10-17 11:43:06	1280	40.7±15.0	172.6±14.8	177.3±14.9	38.4±2.4
HD 10162	F0IV	100.2	3.3561	2015-10-17 14:50:26	1280	-93.8±23.6	107.8±19.7	142.9±21.9	65.5±4.4

around zero for the polarized light to be approximately 200 ppm for the system. This is rather more than the values we found for HD 189733, but appropriate to the measurement of this system (see Table 3).

At the distance of WASP-18 the model described in Cotton et al. (2016) is informed by very little data. This distance is near the wall of the local hot bubble, a region of space with a greater dust density, imparting greater interstellar polarization (Leroy 1999). So, as a further test of the level of interstellar polarization we observed three stars near to WASP-18 in the same bandpass. These stars were chosen for: having spectral types not known to be intrinsically polarized, their brightness, and their proximity to WASP-18. Table 5 gives the results of these observations. The differences between the control stars, likely due to the patchiness of the interstellar medium, prevents us from precisely determining the interstellar polarization for WASP-18 directly from these measurements. However, it is clear the control stars have a similar magnitude and polarization position angle to that which may be calculated from Z_q and Z_u in Table 3 ($Z_p = 199.7 \pm 5.8$ ppm, $Z_{PA} = 56.1 \pm 0.9$ deg). Thus it is very likely that the majority of the constant polarization signal is due to interstellar polarization.

Circumstellar dust can also produce a constant polarization signal (Kolokolova & Kimura 2010; Cotton et al. 2016; Marshall et al. 2016) and while its signal is typically assumed to be constant, the characterization and consideration of the influence of debris is vital to characterizing planets both in polarized and unpolarized observations (Roberge et al. 2012). WASP-18 likely does not have any significant circumstellar debris, although even zodiacal dust can contribute a small degree of polarization offset. In Figure 3 we show the spectral energy distribution (SED) fit to photometry including the Optical BV (Hipparcos catalogue, (Perryman et al. 1997)), and near-infrared 2MASS JHKs (Skrutskie et al. 2006), and WISE mid-infrared (Wright et al. 2010). The same model stellar photosphere from the ATLAS9 database used in our polarization models of transit (Section 3.5) and tides (Section 3.6) is placed on the image with these data points. The spectral energy distribution (SED) shows no significant excess across the available wavelength range although constraints at and beyond the mid-infrared ($\geq 20\mu\text{m}$) are weak.

Furthermore we might consider that such an irradiated planet might be experiencing atmospheric loss which could contribute to the polarization signal. While other hot Jupiters have shown evidence of these processes (e.g. HD 189733b (Bourrier et al. 2013), HD 209458b (Linsky et al. 2010), WASP 12b (Haswell et al. 2012)) the mass loss estimates of WASP-18’s hot Jupiter are quite small based on the X-ray emission of its host star (Salz et al. 2015). Contributions to variations in polarization from asymmetries in the planet’s atmosphere, such as cyclonic spots and localized hazes, are expected to produce signals of only a few percent (Karalidi et al. 2013), which is negligible for this planet. Asymmetries in polarization from the hot spots observed on some hot Jupiters are currently poorly understood.

3.4. Stellar Activity and Interactions

A very young star might be expected to have activity leading to polarized light signals from abundant starspots upsetting the symmetry of the star’s atmosphere (Kostogryz et al. 2015) or from differential saturation from Zeeman splitting of spectral lines (see Cotton et al. (2017a)). The age of the WASP-18 system is poorly constrained, but likely to be fairly young (Hellier et al. 2009; Brown et al. 2011). Isochrone fitting for the star suggests it is 600 Myr, however the non-detection of X-rays from a star that old is unusual, furthermore the slow rotation of the star would imply it is much older than other metrics would suggest. Interactions with the massive and closely orbiting planet could prematurely slow the star, stealing away rotational energy. It is also possible that the planet disrupts the stellar magnetic dynamo created within the star’s thin convective layers, reducing the mixing and allowing the detected lithium—an indication of youth—to last longer. Whatever the star’s age may be, its current state as indicated from studies of Ca II H and K lines and X-ray activity suggests it is relatively inactive, likely with a weak magnetic field, producing few star spots and not interacting with its planet’s magnetic field (Miller et al. 2012).

The interactions between the magnetic fields of closely orbiting hot Jupiters and their stars are possible sources of polarized light (Bott et al. 2016; Fares et al. 2010; Walker 2008). However, in the WASP-18 system the star is expected

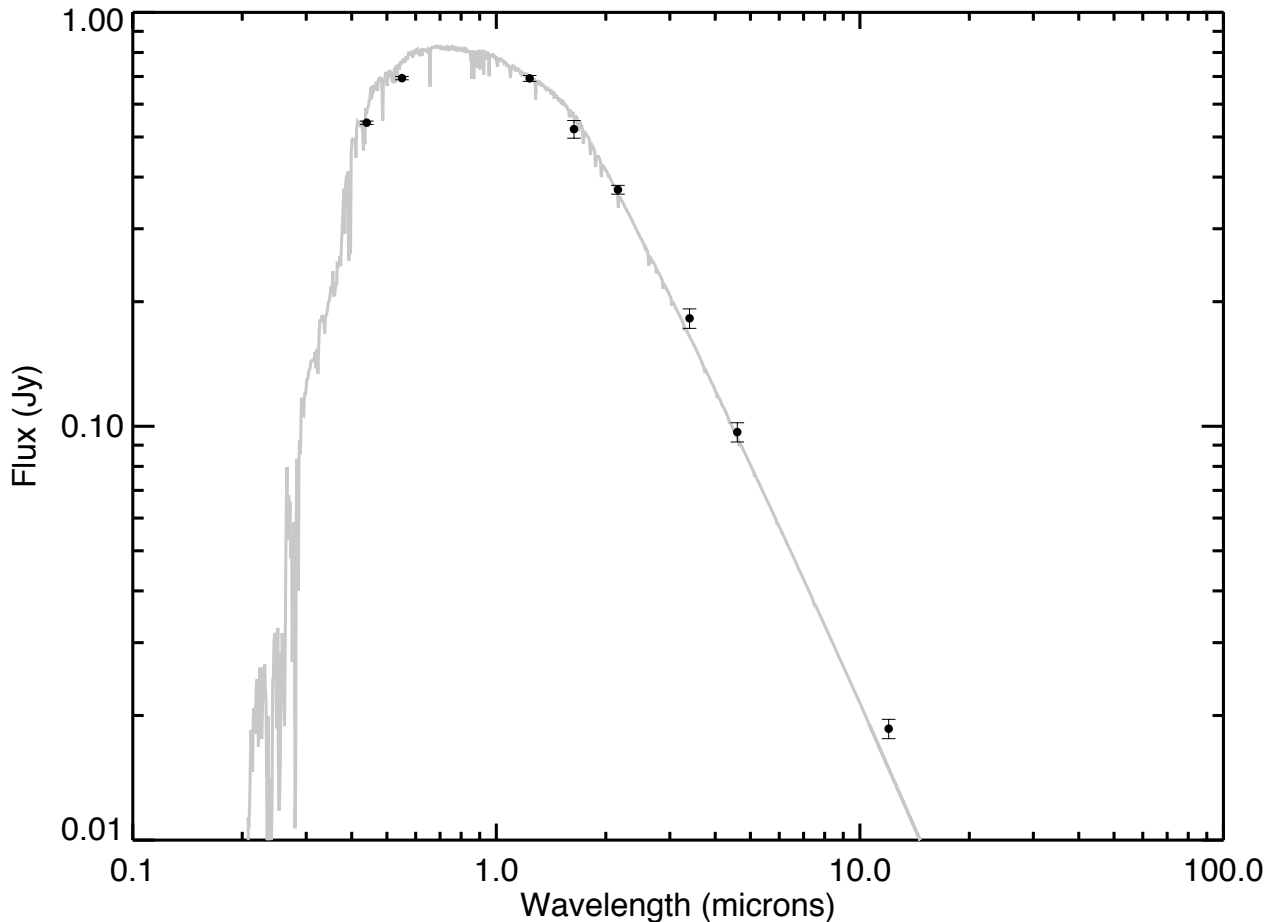


Figure 3. An SED (spectral energy distribution) fit to combined photometry of WASP-18. Black data points are literature values compiled from optical, near-infrared and mid-infrared catalogues, with 1-sigma uncertainties. The grey line denotes the stellar photosphere model. Note that the photosphere model has not been scaled to fit the photometry - see text for details. No significant excess emission is detected at any wavelength.

to have a weak magnetic field due to tidal interactions with the planet disrupting convection which in turn disrupts the stellar dynamo (Pillitteri et al. 2014).

3.5. Transit Polarimetry

Our observations cover two transits observed on 2015 October 19th and 20th. During the transits we reduced the integration times of our observations to attempt to detect any polarimetric signals due to the transit. The reduced integration time has the effect of increasing the uncertainty of these points to around 50 ppm or higher.

The observations within the transit are shown in Figure 4. These observations show increased scatter compared with the longer, out-of-transit integrations, but this is consistent with the increased uncertainties. There is no indication of polarization variability resulting from the transit.

Polarization during transit is expected to be produced as a result of scattering in the stellar atmosphere. Normally this polarization is perpendicular to the radius vector and increases toward the limb of the star. The symmetry of a spherical star will cause the polarization to integrate to zero over the whole star. However, the occultation by a planet will break this symmetry and result in net polarization, which is expected to be largest when the transiting planet is near the limb of the star. The effect is analogous to the Chandrasekhar Effect originally predicted for hot stars in eclipsing binaries (Chandrasekhar 1946) and observed in the case of Algol (Kemp et al. 1983). The light transiting

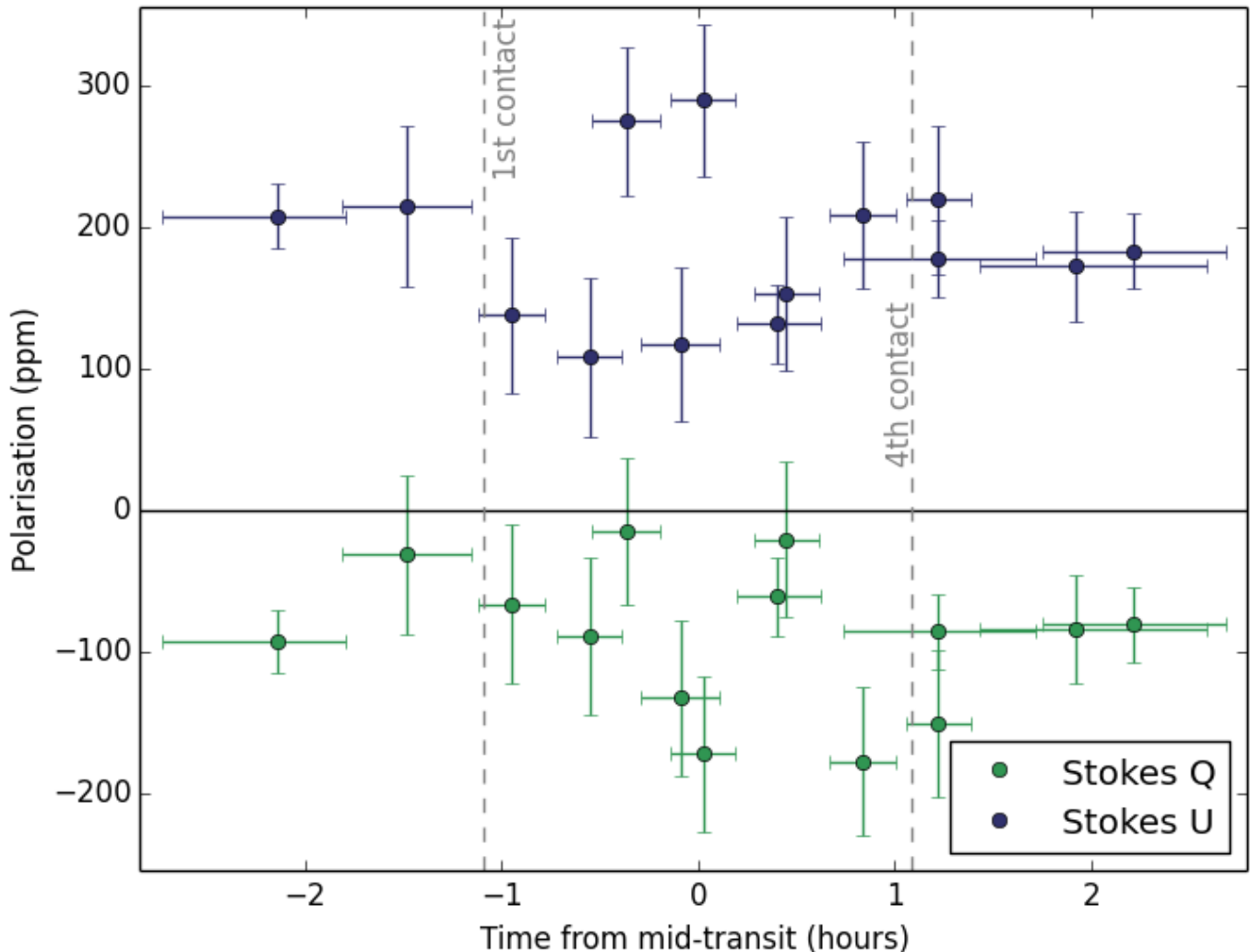


Figure 4. HIPPI measurements of the polarized light from the WASP-18 system around and through transit (1st to 4th contact) centered on mid-transit. Here the data are plotted on the same axes. The vertical error bars are the true error, while the horizontal error bars show the duration of the integration (start to stop time of observation). There is more noise in the transit than outside of it because the exposures are shorter.

through the planet’s atmosphere is also affected by polarization (de Kok & Stam 2012) but for this geometry of a large gas giant very near its star, the stellar contribution is likely dominant.

This transit polarization effect has been investigated for planets transiting cool stars by Carciofi & Magalhaes (2005) and Kostogryz et al. (2011). Kostogryz et al. (2015) have calculated the transit polarization for a range of transiting planets, and shown that the size of the effect increases for lower stellar temperatures, lower gravities, and larger planet to star radius ratios, with the effect reaching up to 10 ppm or more at 400 nm in the most favourable cases. However, WASP-18 is outside the range of parameters considered in that study.

We have calculated new models for transit polarization over a wider range of stellar types, using an adaptation of the modelling methods used by Cotton et al. (2017b) to calculate the polarization due to the rotational oblateness of Regulus. We start with an ATLAS9 stellar atmosphere model. For the WASP-18 case we use a model for $T_{eff} = 6368$ K and $\log g = 4.37$ (the stellar parameters of WASP-18 according to Torres et al. 2012) based on the solar abundance grid of Castelli & Kurucz (2004). We then calculate the emergent specific intensity and polarization as a function of wavelength and viewing angle ($\mu = \cos \theta$, where θ is the local zenith angle) using the SYNPEC/VLIDORT code. This is a version of the SYNPEC spectral synthesis code (Hubeny et al. 1985) which we have modified to do polarized radiative transfer using the Vector Linearized Discrete Ordinate Radiative Transfer (VLIDORT) code of Spurr

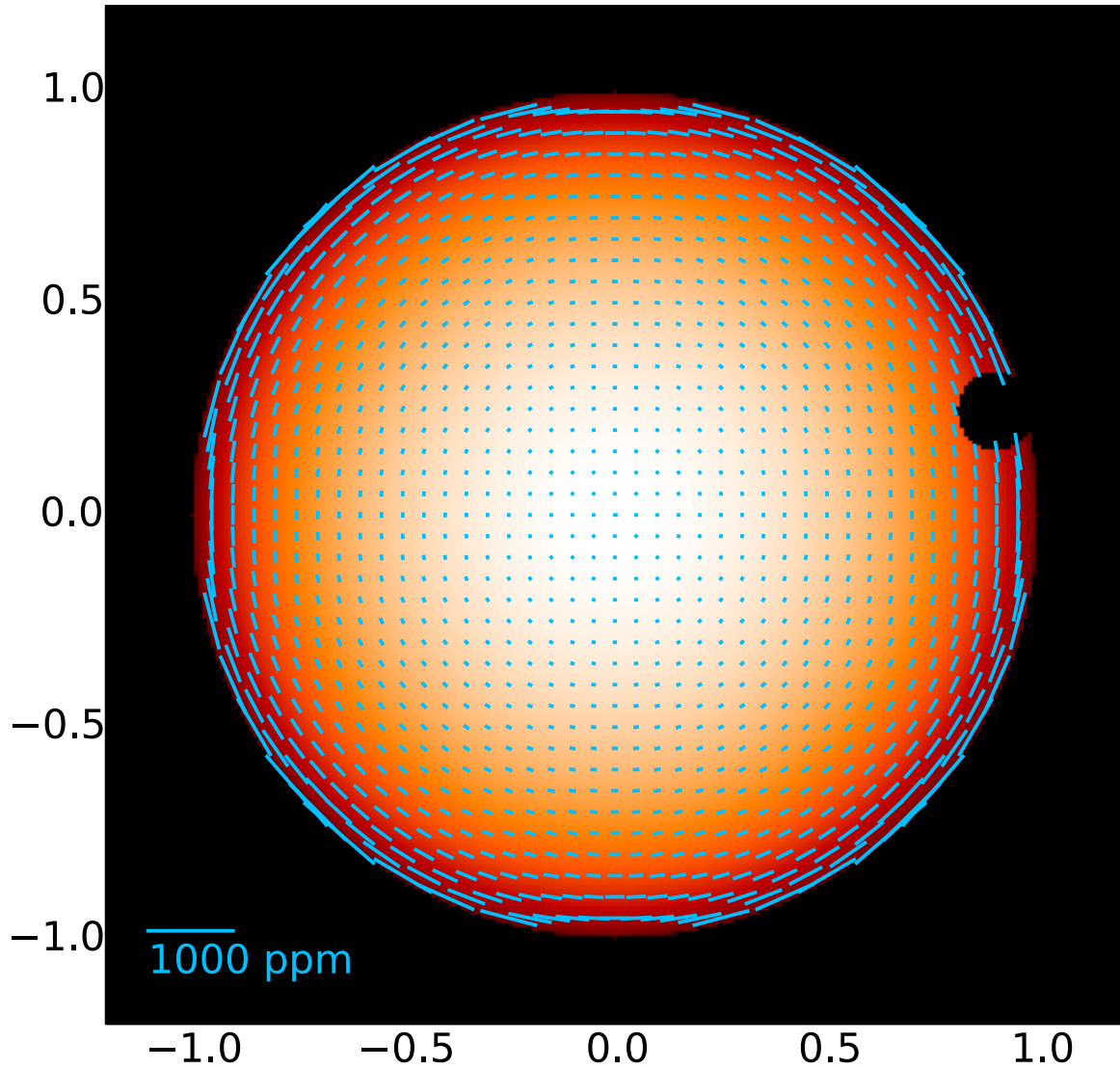


Figure 5. Example of polarization transit modelling. The intensity distribution and overlaid polarization vectors at 440 nm wavelength are shown for a WASP-18 model with a transiting planet near the phase that produces the maximum polarization.

(2006). The calculations include the polarization due to Thompson scattering from electrons (most important in hot stars) and Rayleigh scattering due to H and He atoms and H₂ molecules (important in cool stars).

We then set up a grid of “pixels” covering the observer’s view of the star and spaced at 0.01 of the stellar radius. For each pixel we determine the viewing angle μ and then interpolate in our set of SYNSPEC/VLIDORT calculations to determine the intensity and polarization spectrum for that pixel. The resulting data provide a map of the intensity and polarization distribution across the star at each wavelength. To model a transit we remove from the map those

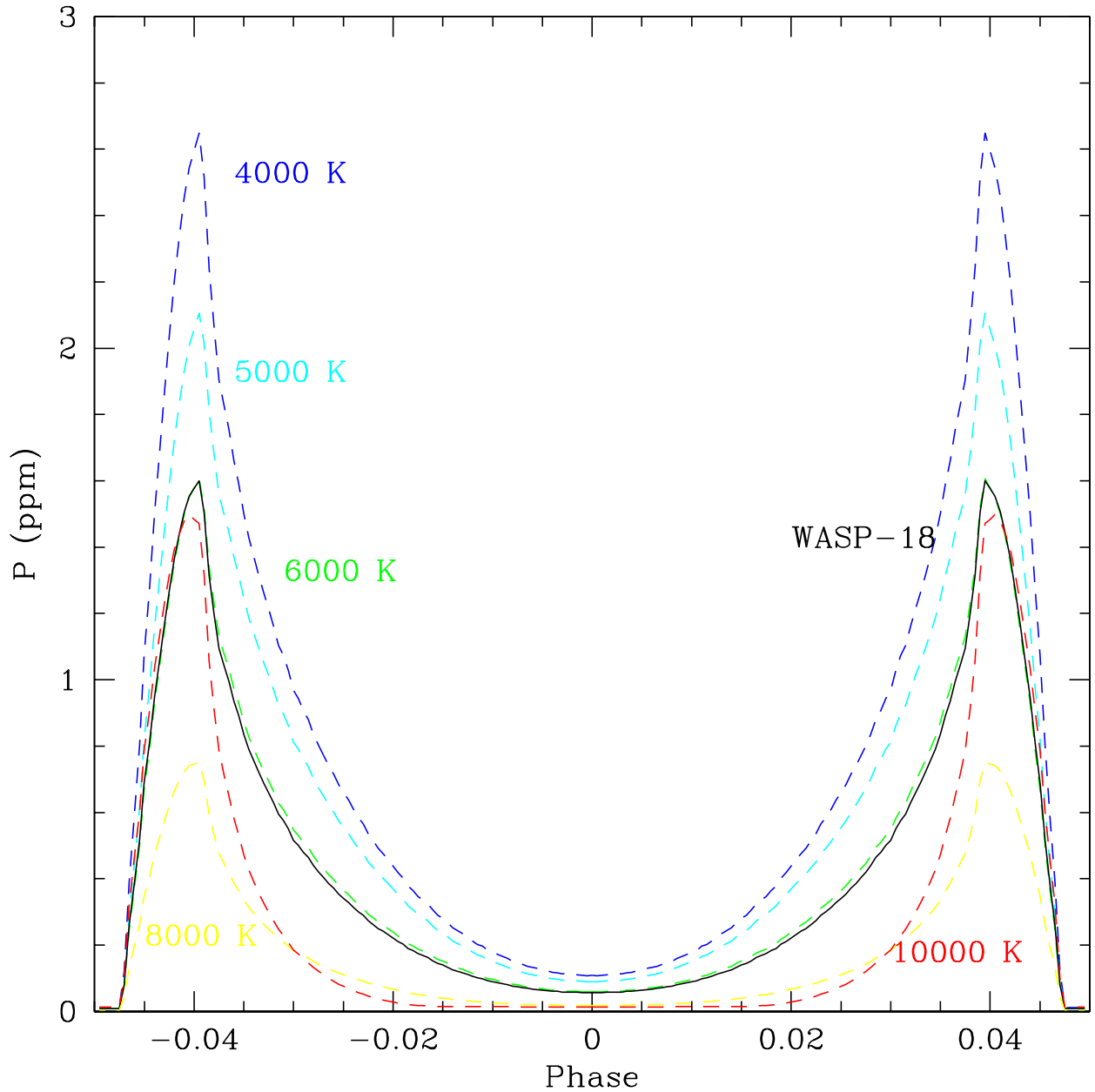


Figure 6. Modelled polarization curves for the WASP-18 transit (solid line) at a wavelength of 440 nm. Dashed lines show models for the WASP-18 transit geometry but for stellar atmosphere grid models of different temperatures at $\log g = 4.5$.

pixels that are occulted by the planet and sum the remaining pixels to give the integrated intensity and polarization at that point during the transit¹. An example of the resulting data is shown in Figure 5.

For the results presented here we have modelled the transit geometry appropriate to WASP-18b using an inclination of 86 degrees (the inclination will change the shape of the curve but not the maximum polarization) and a planet/star radius ratio of 0.0913. Figure 6 shows results for the polarization variation during transit for the WASP-18 model

¹ Since we know the polarization over the whole star should integrate to zero, it is equivalent to integrate only the pixels occulted by the planet and then reverse the sign. In practice we use both methods as a consistency check.

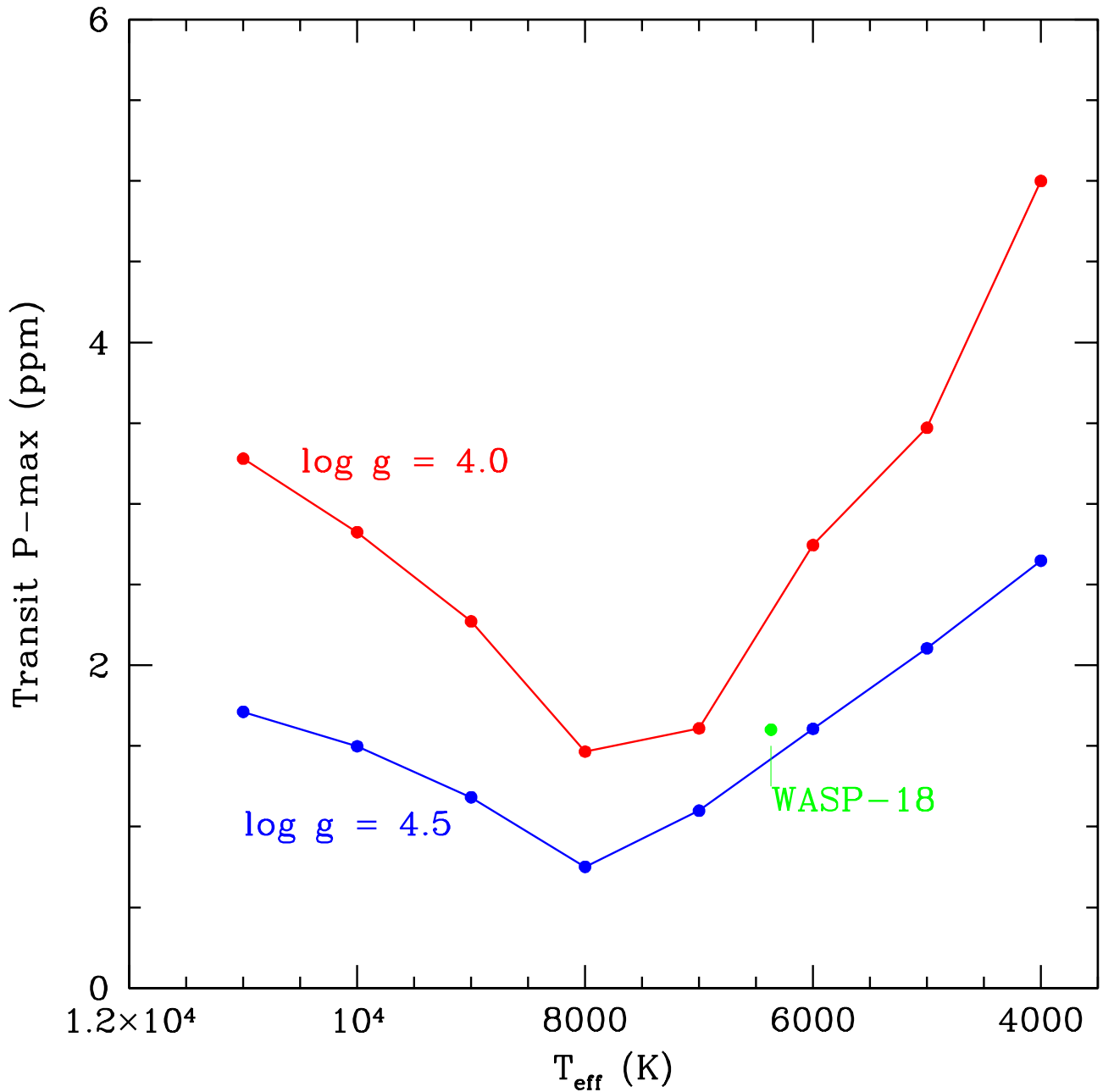


Figure 7. Maximum polarization during transit (at 440 nm) as a function of stellar effective temperature and gravity for the WASP-18 - WASP-18b radius ratio. Grid models with $\log g$ of 4.0 and 4.5 are shown, while the WASP-18 model with $T_{\text{eff}} = 6368$ K and $\log g = 4.37$ is indicated by the green dot. The noise in the transit in Figure 4 is significantly greater than this.

shown by the solid line. The polarization amplitude is 1.6 ppm. Given that our transit observations have errors of ~ 50 ppm, and that the scatter in the data is particularly large during the short observations taken during transit (see Figure 5), it is unsurprising that we did not detect any effect.

In addition to the model specific to WASP-18 we have investigated the variation of the transit signal with stellar type by running models for the WASP-18 transit geometry but substituting stellar atmosphere models taken from the Castelli & Kurucz (2004) grid with T_{eff} from 4000 K to 11000 K and $\log g$ of 4.5 and 4.0. Some of these models are shown as dashed lines on Figure 6, and in Figure 7 we show the maximum polarization during a transit as a function

of temperature and gravity. The results show that the transit polarization signal reaches a minimum at about 8000 K, but then starts to increase again at higher temperatures, which is due to the increasing importance of electron scattering in hotter atmospheres.

The recent discovery of transiting planets such as KELT-9b (Gaudi et al. 2017) which orbits a B9.5-A0 star of 10170 K shows that the transit polarization effect may be observable in hotter stars as well as cool stars.

3.6. Tidal Distortion

Another way of breaking the polarization symmetry of a star is through tidal distortion of the star by the planet and the planet by the star in turn. This has been suggested as a possible polarization mechanism for exoplanet systems (e.g. Hough & Lucas 2003) but estimated to be a small effect in most cases. WASP-18b is, however, an extreme case in view of the mass of the planet, and the closeness of the planet to the star.

We can model the polarization produced by tidal distortion of the star using the same methods as those in Cotton et al. (2017b) and in Section 3.5 above. We use the formulation of Wilson & Devinney (1974) as updated by Wilson (1979) to describe the geometry of a tidally distorted star including the case of non-synchronous rotation. This allows us to determine the shape of the star, the variation of effective gravity across its surface, and the viewing angle μ and rotation angle ξ at any point on the star for a given inclination and phase angle. We can then derive intensity maps and integrated polarizations using the same methods as in Cotton et al. (2017b). We use a set of ATLAS9 models covering the required range of gravities and temperatures. We calculate the polarization and intensity for these models using SYNPEC/VLIDORT and interpolate in between them to obtain results for each “pixel” across the star. We assume effective temperature and gravity are related through the von Zeipel gravity darkening law $T_{eff} \propto g^\beta$ where $\beta = 0.25$ (Von Zeipel 1924). According to Espinosa Lara & Rieutord (2012) this is a good approximation for most binary parameters.

For WASP-18 the mass ratio $q = M_P/M_S$ is 0.0078. We consider first the extreme case of a star large enough to fill its Roche lobe. This requires a star more than twice as large as WASP-18. In a system with such an extreme mass ratio the star has an oblate shape arising from its phase locked rotation, and the tidal distortion mostly shows up in the region close to the L_1 point where there is a low gravity region, forming a cold spot on the star (due to gravity darkening) immediately below the planet. This can be seen in Figure 8. The cold spot moves across the star as the phase angle changes and produces polarization similar to that for the transiting case with the polarization being highest when the cold spot is near the limb which occurs at 60-70 degree phase angles. For the planet, because the polarized light is reflected light, the oblateness of the planet does not have as great an effect on the path geometry and hence we can expect this is an even smaller, negligible effect.

The resulting phase variations are shown in Figure 9. The largest polarization effect arises from the oblateness of the star. This produces a phase independent polarization of 36 ppm at 440 nm for the Roche lobe filling case which is far more extreme than the actual estimated oblateness of WASP 18. The changing position of the cold spot with phase produces a phase dependent polarization of a little under 4 ppm for the Roche lobe filling case.

In the actual case of WASP-18 the star is much smaller than the Roche lobe, and it is also apparent from the measured $v \sin i$ that it is not synchronously rotating. In our model we consider a star rotating 5 times slower than the orbital period. For such a star there is little rotational oblateness, but low-gravity cold spots can be seen on the sides of the star towards and away from the planet. However, the contrast in gravity between the cold spots and the rest of the star is now very small as can be seen in the top right panel of Figure 8. The resulting polarization phase curve (Figure 9) for such a star has an amplitude of only about 0.1 ppm, far below our measurement errors.

Thus it seems that even for this relatively extreme case (as compared with other hot Jupiters) the tidal effects do not significantly contribute to observed polarization, and this effect can be safely ignored in future studies of exoplanet polarization at least until the sensitivity of polarimeters is improved.

3.7. Forward Polarimetric Model

We have modelled the reflected light polarization of WASP-18b using the VSTAR (Versatile Software for Transfer of Atmospheric Radiation) code (Bailey & Kedziora-Chudczer 2012) which has been updated to model polarization as described by Bailey et al. (2018). The atmospheric model we used for WASP-18b has been used to fit the emission spectrum of the planet determined from secondary eclipse observations with HST, Spitzer and ground-based telescopes as described by Kedziora-Chudczer et al. (2018). The model uses a temperature profile with an inversion above 0.1 bar, and assumes solar metallicity and equilibrium chemistry. Absorption due to molecular and atomic lines of 16 species

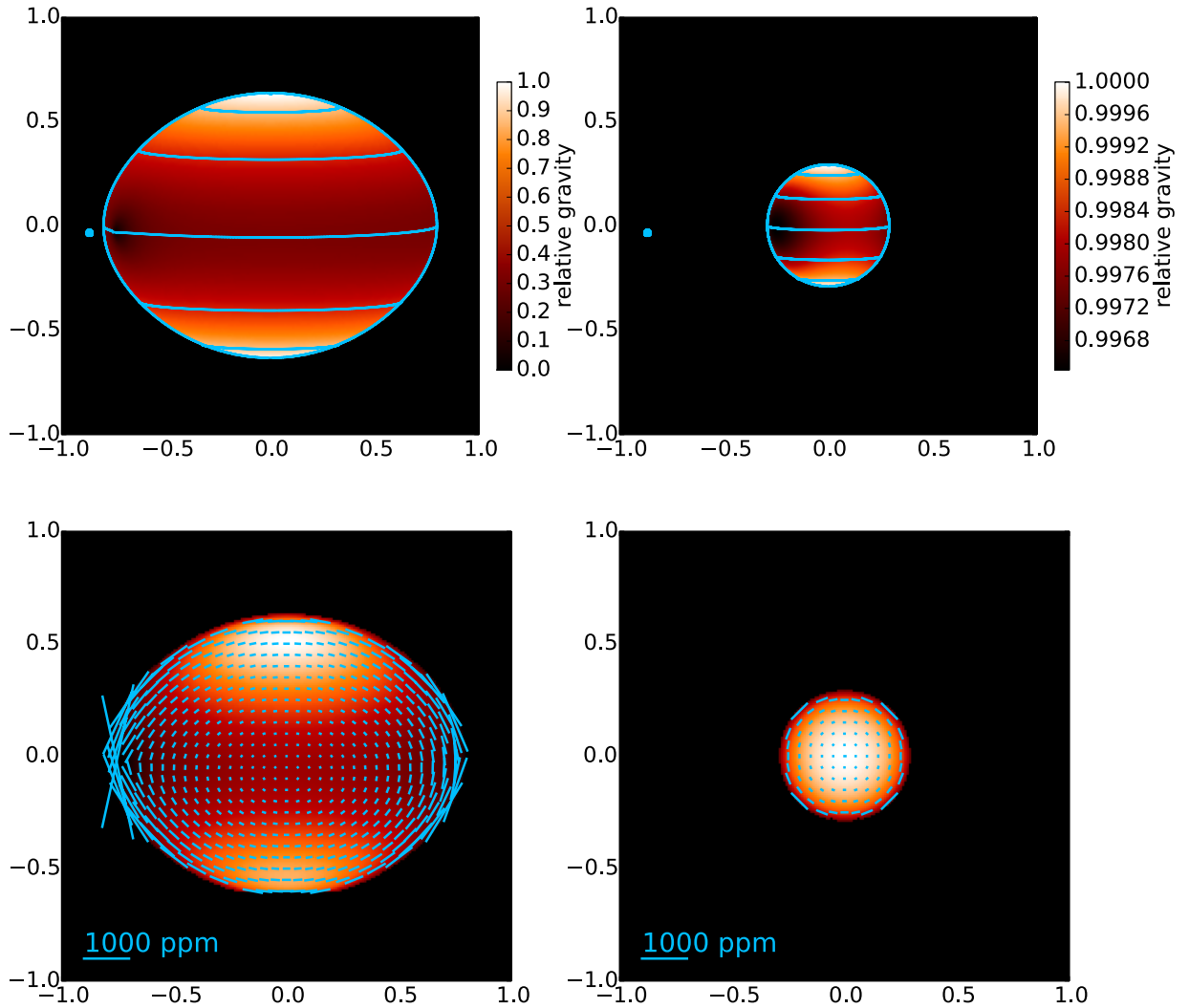


Figure 8. Models for polarization due to tidal distortion. The inclination is 86 degrees and the phase angle is 60 degrees. The left panels show results for a star large enough to fill its Roche lobe, while the right panels are for the actual WASP-18 star size and a rotation rate 5 times slower than the orbital period. At the top is shown the shape and effective gravity distribution over the star. For the Roche lobe filling case there is a low gravity region near the L1 point which results in a cold spot below the planet. This results in an asymmetry that produces a phase dependent polarization effect. For the actual WASP-18 cold spots are seen on either side of the star, but the contrast in gravity is now very small. The lower panels show the resulting intensity distribution and overlaid polarization vectors for a wavelength of 440 nm. The blue dot in the top panels is the planet shown at its correct position.

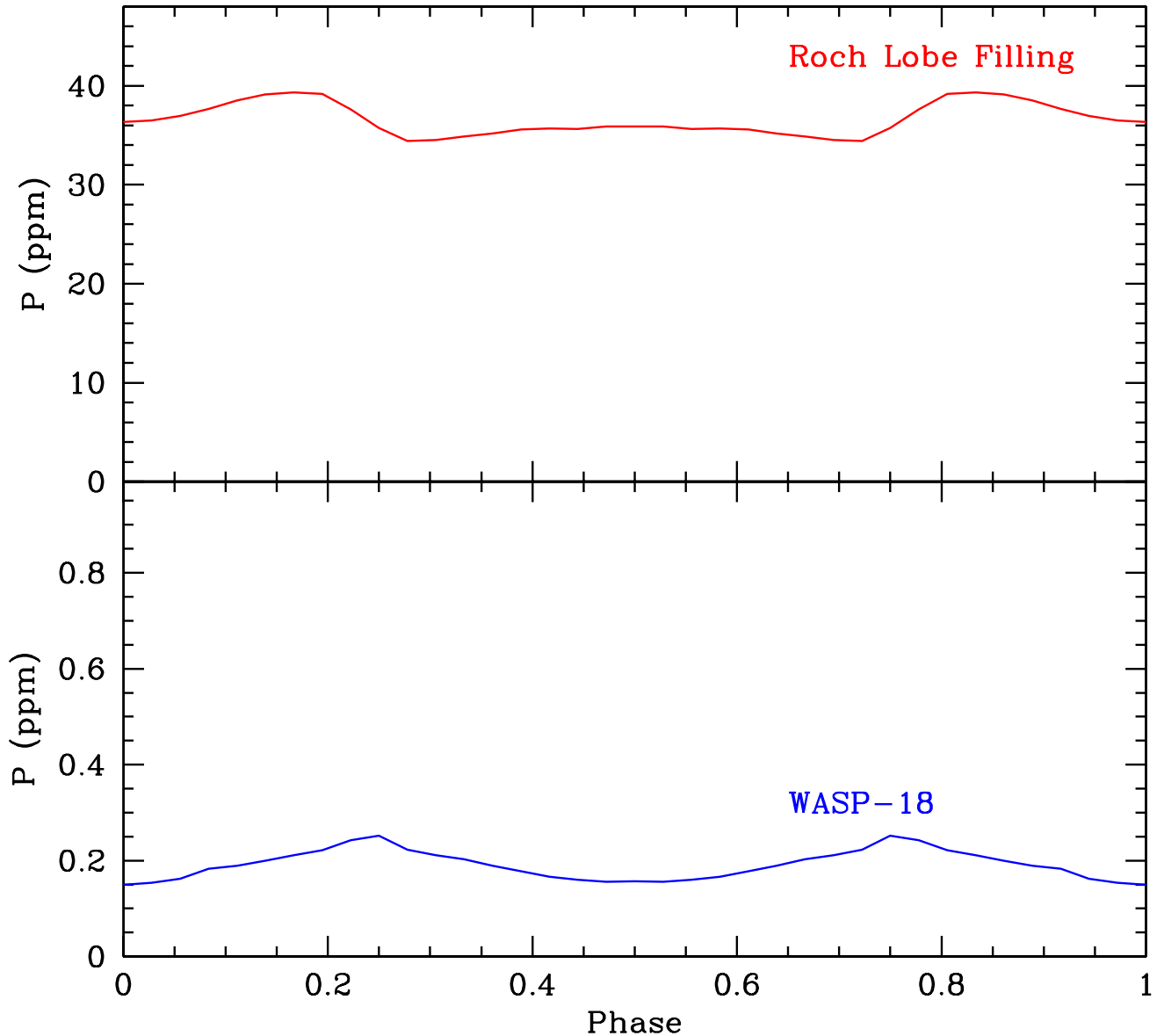


Figure 9. Modelled polarization phase curves at 440 nm due to tidal effects for the two cases shown in Figure 8. The variation in polarized light from this effect for WASP-18 is below HIPPI’s sensitivity.

(H_2O , CO , CH_4 , CO_2 , C_2H_2 , HCN , TiO , VO , Na , K , Rb , Cs , CaH , CrH , MgH and FeH) is included. Additional opacity sources are Rayleigh scattering due to H , He and H_2 , $\text{H}_2\text{-H}_2$ and $\text{H}_2\text{-He}$ collision-induced absorption, and bound-free and free-free absorption from H , H^- and H_2^- .

To calculate the reflected light polarization from this model we use the VLIDORT vector radiative transfer code (Spurr 2006) to solve the polarized radiative transfer equation at a grid of pixels spaced across the visible disk of the planet. We then integrate over these pixels to obtain the disk-integrated intensity and polarization from the planet. The methods and a number of verification tests are described in detail by Bailey et al. (2018).

Table 6. A comparison of the albedos and maximum polarization signal for the models plotted in Figure 10.

Model	Geometric Albedo	Max polarization (ppm)
Clear	0.00090	0.17
Rayleigh clouds ($\tau = 10$)	0.673	58.7
Rayleigh clouds ($\tau = 1$)	0.301	45.3
Enstatite clouds ($\tau = 1$)	0.214	38.7
Corundum clouds ($\tau = 1$)	0.150	28.4

The results for WASP-18b for a wavelength of 470 nm are shown in Figure 10 and summarized in Table 6. For a model with a clear (cloud free) atmosphere, the reflected light from the planet is extremely weak and the corresponding polarization amplitude is only 0.17 ppm. This is because, although polarized reflected light can be produced by Rayleigh scattering from H_2 , the absorption opacities (due, for example, to TiO and H^- free-free) are so dominant at this wavelength that very little scattered light is seen. Some of these absorbers, such as H^- free-free are anticipated to be a substantial part of the atmosphere (Arcangeli et al. 2018). Although the scattered light shows almost 100% peak polarization (since predominantly single scattering is seen) it remains a very small fraction of the light from the star. The extreme low level of reflected light is different to the case of the cooler planet HD 189733b considered by Bailey et al. (2018) where a polarization of 7 ppm could be produced in the clear case.

The Rayleigh scattering cross section of H_2 depends strongly on the wavelength with the polarization from H_2 (which is the primary source of polarization in the clear atmosphere case and the dominant gas in the other cloud cases) increasing towards the UV, however this is a small effect beyond the sensitivity of our measurements. To quantify this effect, we compared the five atmospheric models—clear atmosphere (H_2 dominated), corundum, enstatite, and two “pure-Rayleigh” scattering clouds—using our bandpass model in three different spectral bands. Those bands are: clear pass, which was used for the observations presented here; 500SP, which is HIPPI’s primary blue filter used for the HD 189733b observations (Bott et al. 2016); and Johnson U, as an example of a U-band filter. In the clear atmosphere case the measurements of polarization are estimated to be 0.18, 0.22, and 0.25 ppm for the three bandpasses respectively. In the other cloud models the values vary by a few parts-per-million at most, with efficiencies of 84%, 80.2% and 39.5% in Clear, 500SP and Johnson U respectively. In cases where there is an increase in polarization it is not significant enough to overcome the loss in stellar flux at bluer wavelengths. Multi-band observations could help to distinguish the stellar effects from those of the planet particularly if the star appears to be active ((Cotton et al. 2018) note that WASP 18 is not), however, for the measurements presented here, our bandpass model suggests those variations are beyond our sensitivity.

Substantial reflected light and polarization can be achieved by including a cloud layer high in the atmosphere. As discussed by Bailey et al. (2018) the highest polarization is achieved with an optically thick Rayleigh scattering atmosphere. Our model with an optical depth $\tau = 10$ of pure Rayleigh particles produces a polarization amplitude of 58.7 ppm. These can be thought of as idealized small (compared with the wavelength) non-absorbing particles with a single-scattering albedo of one and a Rayleigh phase function. A similar model with $\tau = 1$ gives 45.3 ppm. Models using 0.05 micron radius particles of enstatite ($MgSiO_3$) and corundum (Al_2O_3) give slightly lower polarizations (here the particles are “Rayleigh like” but include significant absorption unlike our “pure Rayleigh particle” clouds). Both these species—enstatite and corundum—have condensation temperatures too low for the atmospheric temperature profile we are using. However the possibility that clouds form on the colder night-side and are transported to the day-side is considered by Kedziora-Chudczer et al. (2018).

The most realistic scenarios here do not exceed the 40 ppm signal ruled out by the polarimetric observations in this paper. In fact, most cloudy scenarios except Rayleigh scattering particles with a greater optical depth, and certainly a dark clear atmosphere, may produce signals below this threshold.

The model results shown in Figure 10 and Table 6 are monochromatic calculations at 470 nm, while our actual band is quite broad. If polarization varies strongly with wavelength these calculations may not accurately represent what we should observe in our broad band. To test this effect we carried out a full set of wavelength dependent polarization models over the range 300 nm to 1000 nm for one phase angle, 67 degrees, near where the observed polarization peaks, and used our bandpass model to determine the integrated polarization we should observe over the band for each of the models shown in Figure 10 and Table 6. The polarizations at this phase are 0.18 ppm for the clear model, 59.0 ppm and 41.9 ppm for the two Rayleigh models, and 36.3 ppm and 26.3 ppm for the enstatite and corundum models

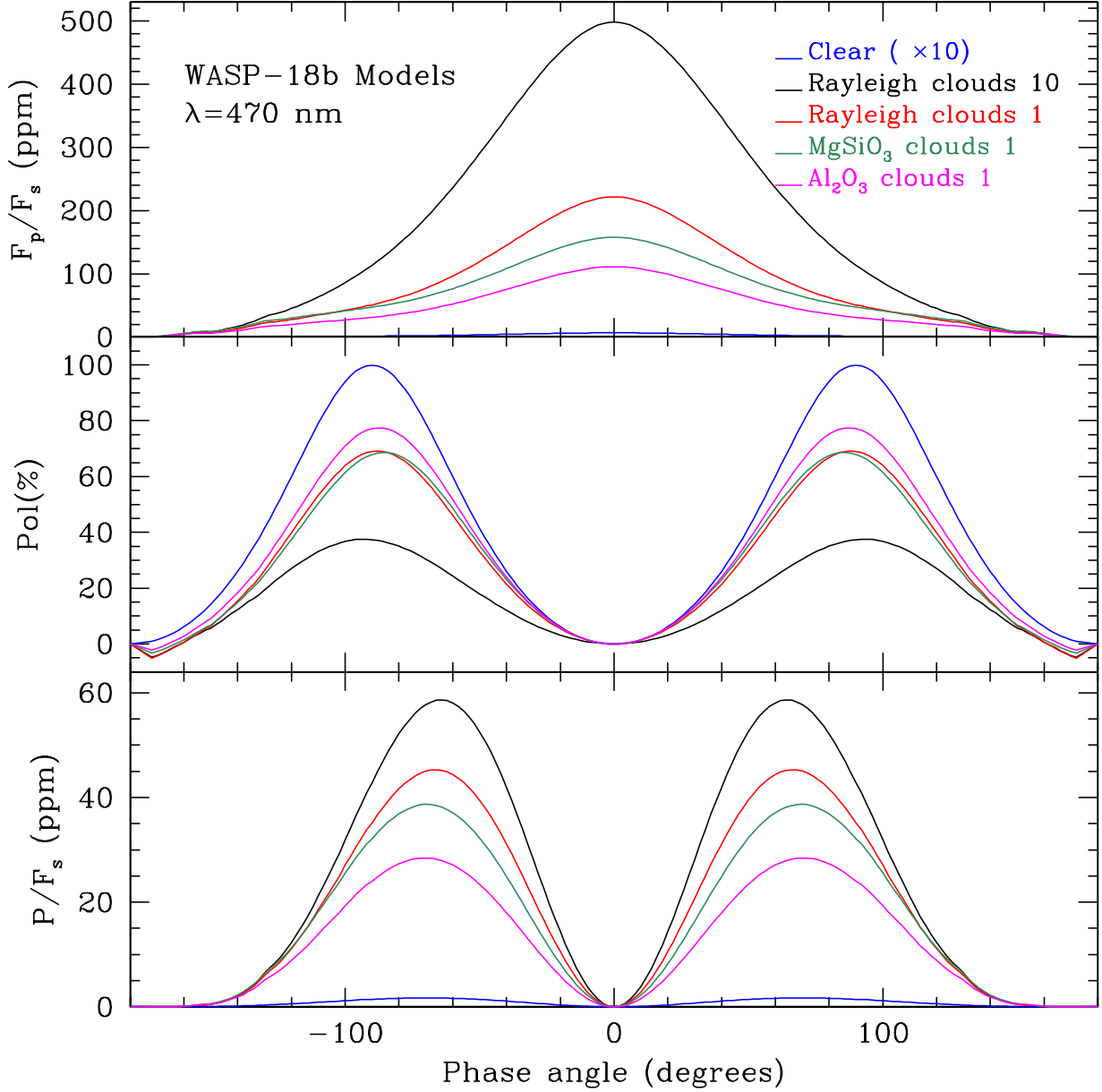


Figure 10. Predictions of the anticipated polarized light curves based on models in [Kedziora-Chudczer et al. \(2018\)](#) based on new Gemini observations of the system. These models are for a clear atmosphere and various cloud layers. The upper panel is the light reflected from the planet as a fraction of that from the star. The middle panel is the percentage polarization of the light reflected from the planet. The lower panel is the polarization as a fraction of the light from the star and corresponds to the quantity we actually observe. The cloud models are for Rayleigh scattering clouds with optical depths 10 and 1, and clouds with optical depth 1 composed of $0.05 \mu\text{m}$ radius enstatite (MgSiO_3) and corundum (Al_2O_3) particles. The clear model has been scaled up by a factor of 10 to be visible at all in the top and bottom panels.

respectively. These are quite close to the values at this phase angle seen in [Figure 10](#), indicating that no major error is introduced by using a monochromatic model to represent our observations.

4. DISCUSSION

Typically hot Jupiters are selected for polarimetric observation based on the large size of their scattering disk and their proximity to their host star (and hence the amount of light to be scattered). WASP-18b is an extreme

example of this as it orbits especially close to an F-type star. We are able to produce a constraint on the polarimetric signal from the planet at no greater than 40 ppm from observation, which rules out atmospheres with optically thick ($\tau = 10$) Rayleigh scattering clouds, and detect an offset likely primarily due to the interstellar medium. We were unable to detect a polarized light signal modulated by the planet WASP-18b system in spite of its advantages as a candidate. Possible explanations for this non-detection include a detectable signal just outside of our sensitivity given our observing time, or the planet having a low albedo.

Extended observations or observations with a larger light collecting area can drive down our noise so that we are limited by HIPPI's precision. For HIPPI or any other high precision polarimeters reaching this sensitivity, obtaining errors in the parts-per-million range could open up the possibilities of determining the cloud species, confirming a dichotomy of albedos on hot Jupiters, and exploring the other phenomena such as the transit. For stars that are more active than WASP 18, observing the system in multiple wavelength bands may help disentangle the stellar contributions from effects like line-blanketing from stellar activity from the planetary signal.

The seminal paper on which estimates of the polarized light signals of hot Jupiters are typically based, Seager et al. (2000), concentrated on planets with temperatures half of what has been measured for WASP-18b (Nymeyer et al. 2011) and modelled atmospheres with clouds or strong Rayleigh scattering. Some hot Jupiters may have dark atmospheres without reflective clouds. WASP-18b is likely one of them considering its high temperatures and the absorbing species likely present in its atmosphere (Burrows et al. 2008; Fortney et al. 2008; Zahnle et al. 2009; Knutson et al. 2010). For a super hot giant like WASP-18b the atmosphere may be clear on the day-side unless mixing is able to transport clouds from the nightside (Kedziora-Chudczer et al. 2018). Nymeyer et al. (2011) found from secondary eclipse observations that the planet is far brighter in infrared than the predicted equilibrium temperature requiring it to have a near-zero albedo and inefficient energy transport between the night- and day-sides.

Therefore, a non-detection of polarized light from this exoplanet should not be regarded as a suggestion that such signals do not exist at the levels predicted by Seager et al. (2000). Rather more time for polarimeters capable of detecting at the parts-per-million level, or larger collecting areas, would expedite and enable polarized light detection and characterization of some hot Jupiters, while some other hot Jupiters might lack the thick polarizing or high altitude clouds that would produce a larger signal. Even in cases of cooler planets which might more readily form condensates, the planets may sometimes be dark enough to only produce signals at a few parts-per-million.

In the case of HD 189733b the limits placed on the polarized signal from Bott et al. (2016) were a good match to the observations of secondary eclipse in non-polarized photometry in blue as the planet is a deep dark blue color. In the case of WASP 18b, the color was not known at the time the observations began and relatively less was constrained about its atmosphere than in the HD 189733b case. The low polarimetric signals from clouds as shown in Figure 10 could potentially be observed on a larger telescope, but they are not anticipated to form on the dayside of the planet and would require mixing (Kedziora-Chudczer et al. 2018) to transport them there, although secondary eclipse measurements suggest the planet is quite dark on the dayside (Nymeyer et al. 2011). Other hot Jupiters in longer orbits or around cooler stars may be better objects for polarimetric study despite a decrease in incident flux particularly in blue, if they are able to produce reflective clouds.

The apparent darkness of the planet's dayside from both these polarimetric and previous photometric studies, and Nymeyer et al. (2011)'s finding that there likely is little, if any, energy redistribution from the dayside to the nightside of the planet suggest mixing is not bringing substantial clouds to the dayside. The clouds modelled here and in Kedziora-Chudczer et al. (2018) and indeed in much of the literature are based largely on refractive indices sources (e.g Scott & Duley 1996; Koike et al. 1995; Johnson & Christy et al. 1974; Ordal et al. 1988) for solid phases appropriate to some but not all clouds on hot Jupiters; we caution the community in this regard. Whilst we acknowledge that the high temperatures required to obtain optical data of these materials at liquid phases in a lab is difficult and thus is difficult to find, these solid phase clouds will have optical properties different from what would realistically be found on the dayside of these hottest hot Jupiters. The models here that include clouds are only appropriate if substantial circulation bringing clouds from the nightside to the dayside is present on WASP-18b and the nightside reaches temperatures significantly lower than on the dayside (e.g. less than about 2300 K at 1 bar for solid ice clouds of Al_2O_3) and even so, liquid clouds are likely to also be present.

5. CONCLUSIONS

We have described new measurements in linearly polarized light of the hot Jupiter exoplanet hosting system WASP-18, made with the HIPPI polarimeter. The system provides an unusual test case in the form of a high mass hot Jupiter ($M \approx 10 M_J$) orbiting very closely to its star ($p < 1$ day).

Our best fits to a Rayleigh Lambertian phase curve are not changed substantially by the inclusion of transit observations. The best fit to the modulation in the observations is for WASP-18b to orbit with a position angle of 200.3 ± 20.7 degrees and an inclination of 79.2 ± 10.9 degrees, which is in agreement with literature although low values of inclination within that range can be omitted since it is known that the planet transits. With fitted offsets of Z_q and Z_u at -75.2 ± 6.0 ppm and 185.0 ± 5.5 ppm, the best fit to the signal itself is for a polarization of 16.2 ± 10.0 ppm from the planet which is in good agreement with predictions for polarized light signals from hot Jupiters.

The offsets from zero are to the order of those expected from the interstellar medium and are not expected to come from contributions of the star or circumstellar debris.

We find the signal is statistically not differentiable from a best fit to noise: it is possible to produce a fit to noise for signals of this amplitude with this level of sampling. We can, however, with 99% confidence, rule out a detection at the 40 ppm level. Forward models for the expected polarization signal for the planet exceed our 40 ppm limit only for the most extraordinary cases of pure Rayleigh scattering clouds. Models with more realistic cloud particles can produce polarization amplitudes with 26-36 ppm amplitudes which are still well above our best fit polarization amplitude. The most likely reason that we are not seeing a planetary polarization signal is that the atmosphere of WASP-18b is too hot for clouds to form or move to the day-side. A clear atmosphere results in a very low geometric albedo and a polarization well below our detection limits.

Other noise sources and polarization mechanisms were explored. Tides are inflicted on the star and planet in this tight orbit, however we find they are unlikely to produce a detectable signal. We also assess the transit signal in polarized light and find that we do not detect the effects predicted by [Wiktorowicz & Laughlin \(2014\)](#).

This paper serves as a template for the thorough treatment of polarized light signals from exoplanets. The observational approach is promising but relatively novel and so requires the thoughtful treatment of noise sources and combined polarimetric effects. Further observations on an 8-meter class telescope with a HIPPI analogue instrument should produce substantial data points to provide confidence in either a detection under 40 ppm of polarized light from Rayleigh scattering from the planet, or a firm non-detection.

The development of HIPPI was funded by the Australian Research Council through Discovery Projects grant DP140100121 and by the UNSW Faculty of Science through its Faculty Research Grants program. The authors thank the Director and staff of the Australian Astronomical Observatory for their advice and support with interfacing HIPPI to the AAT and during the observing runs on the telescope. The analyses of these observations were reliant upon data from the SIMBAD database and Gaia archive. KMB and VSM acknowledge support from the NASA Astrobiology Institutes's Virtual Planetary Laboratory, funded under cooperative agreement number NAA13AA93A.

Facilities: AAT, UNSW: HIPPI

Software: VSTAR ([Bailey & Kedziora-Chudczer 2012](#); [Bailey et al. 2018](#)), VLIDORT ([Spurr 2006](#)), SYNSPEC ([Hubeny et al. 1985](#))

REFERENCES

- Arcangeli, J., Desert, J.-M., Line, M.R., Bean, J.L., Parmentier, V., Stevenson, K.B., Kreidberg, L., Fortney, J.J., Mansfield, M., & Showman, A.P., *ApJ Letters*, 855, 2, 272
- Bailey J., 2007, *Astrobiology*, 7, 2, 320-332
- Bailey J., Lucas P.W., & Hough J.H., 2010, *MNRAS*, 405, 2570
- Bailey J. & Kedziora-Chudczer, L., 2010, *MNRAS*, 419, 3, pp. 1913-1929
- Bailey J., Kedziora-Chudczer L., Cotton D.V., Bott K., Hough J.H., & Lucas P.W., 2015, *MNRAS*, 449, 3064
- Bailey J., Kedziora-Chudczer L., & Bott K., 2018, *MNRAS*, 480, 1613-1625
- Berdyugina S.V., Berdyugin A.V., Fluri D.M., Piirola V., 2011, *ApJL*, 728, L6
- Bott, K., Bailey, J., Kedziora-Chudczer, L., Cotton, D.V., Lucas, P.W., Marshall, J., & Hough, J.H., 2016, *MNRAS*, 459, 1, pL109-L113

- Bourrier, V., Lecavelier des Etangs, A., Dupuy, H., Ehrenreich, D., Vidal-Madjar, A., Hebrard, G., Ballester, G.E., Desert, J.M., Ferlet, R., Sing, D.K., & Wheatley, P.J., 2013, *A&A*, 551, A63
- Brooks, A., Clarke, D., & McGale, P.A., 1994, *Vistas in Astronomy*, 38, 4, 377-399
- Brown, D.J.A., Collier Cameron, A., Hall, C., Hebb, L., & Smalley, B., 2011, *MNRAS*, 415, 1, pp. 605–618
- Burrows, A., Ibgui, L., & Hubby, I., 2008, *ApJ* 682, 1277
- Carciofi, A.C. & Magalhaes, A.M., 2005, *ApJ*, 635, 570
- Castelli, F. & Kurucz, R.L., 2004, arXiv:astro-ph/0405087
- Chandrasekhar, S., 1946, *ApJ*, 103, 351
- Cotton D.V., Bailey J., Kedziora-Chudczer L., Bott K., Lucas P.W., Hough J.H., & Marshall J.P., 2016, *MNRAS*, 455, 1607
- Cotton, D.V., Marshall, J.P., Bailey, J., Kedziora-Chudczer, L., Bott, K., Marsden, S.C., & Carter, B.D., 2017(a), *MNRAS*, 467, 1, p. 873-897
- Cotton, D.V., Bailey, J., Howarth, I.D., Bott, K., Kedziora-Chudczer, L., Lucas, P.W., & Hough, J.H., 2017(b), *Nature Ast*, 1, 690
- Cotton, D.V., Evensberget, D., Marsden, S.C., Bailey, J., Zhao, J., Kedziora-Chudczer, L., Carter, B.D., Bott, K., Vidotto, A.A., Petit, P., Morin, J., & Jeffers, S.V. 2018, submitted to *MNRAS*
- de Kok, R.J. & Stam, D.M., 2012, *Icarus*, 221, 2, pp.517-524
- Espinosa Lara, F. & Rieutord, M., 2012, *A&A*, 547, A32
- Fares, R., Donati, J.F., Moutou, C., Jardine, M.M., Griemeier, J.M., Zarka, P., Shkolnik, E.L., Bohlender, D., Catala, C., & Collier Cameron, A., 2010, *MNRAS*, 406, 409-419
- Faucher, Th., Rossi, L., & Stam, D.M., 2017, *ApJ*, 842, 41, 18pp
- Fluri, D.M., & Berdyugina, S.V., 2010, *A&A*, 512, A59
- Fortney, J.J., Lodders, K., Marley, M.S., & Freedman, R.S., 2008, *ApJ* 678, 1419
- The Gaia Collaboration et al., 2016, *A&A*, 595, A1, 36 pp.
- Gaudi, S.B., Stassun, K.G., Collins, K.A., Beatty, T.G., Zhou, G., & 55 other coauthors, 2017, *Nature*, 546, 514
- Haswell, C.A., Fossati, L., Ayres, T., France, K., Froning, C.S., Holmes, S., Kolb, U.C., Busuttil, R., Street, R.A., & Hebb, L., 2012, *ApJ*, 760, 1, 79
- Hellier, C., Anderson, D.R., Cameron, A. C., Gillon, M., Hebb, L., Maxted, P.F.L., Queloz, D., Smalley, B., Triaud, A.H.M.J., & West, R., et al, 2009, *Nature*, 460, 1098–1100
- Hough, J.H. & Lucas, P.W., 2003, in Fridlund, M., Henning, T., eds. *Towards other Earths: DARWIN/TPF and the Search for Extrasolar Terrestrial Planets*, ESA SP-539, ESA Publications Division, Noordwijk, p. 11
- Hough J.H., Lucas P.W., Bailey J.A., Tamura M., Hirst E., Harrison D., & Bartholomew-Biggs M, 2006, *PASP*, 118, 1302
- Hubeny, I., Stefl, S., & Harmanec, P., 1985, *Bull. Astron. Inst. Czechosl.*, 36, 214
- Johnson, P.B., & Christy, R.W., 1974, *Phys. Rev. B*, 9, 5056
- Karalidi, T., Stam, D.M., & Guirado, D., 2013, *A&A*, 555, A127
- Kedziora-Chudczer, L., Zhou, G., Bailey, J., Bayliss, D.D.R., Tinney, C.G., & Osip, D., 2018, *MNRAS*, submitted
- Kemp J. C. & Barbour M.S., 1981, *PASP*, 93, 521-525.
- Kemp, J.C., Henson, G.D., Barbour, M.S., Kraus, D.J., & Collins, G.W., 1983, *ApJL*, 273, L85
- Kemp, J.C., Henson, G.D., Steiner, C.T., & Powell, E.R., 1987, *Nature*, 326, pp 270–273
- Knutson, H.A., Howard, A.W., & Isaacson, H., 2010, *ApJ* 720, 1569
- Kolokolova, L. & Kimura, H., 2010, *A&A*, 513, A40
- Koikem C., Kaito, C., Yamamoto, T., Shibai, H., Kimura, S., & Suto, H., 1995, *Icarus*, 114, 203
- Kostogryz, N.M., Yakobchuk, T.M., Morzhenko, O.V., & Vid'machenko, A.P., 2011, *MNRAS*, 415, 695
- Kostogryz N.M., Yakobchuk T.M., & Berdyugina S.V., 2015, *ApJ*, 806, 1, 97
- Linksky, J.L., Yang, H., France, K., Froning, C.S., Green, J., Stocke, J.T., & Osterman, S.N., 2010, *ApJ*, 717, 2, p 1291
- Lucas P.W., Hough J.H., Bailey J.A., Tamura M., Hirst E., Harrison D., 2009, *MNRAS*, 403, 4, pp 1949-1968
- Leroy, J.L., 1999, *A&A*, 346, pp. 955-60
- Marshall, J., Cotton, D.V., Bott, K., Ertel, S., Kennedy, G.M., Wyatt, M.C., del Burgo, C., Absil, O., Bailey, J., & Kedziora-Chudczer, L., 2016, *ApJ*, 825, 2, id.124
- Maxted, P.F.L., Anderson, D.R., Doyle, A.P., Gillon, M., Harrington, J., Iro, N., Jehin, E., Lafrenière, D., Smalley, B., & Southworth, J., 2013, *MNRAS*, 428, pp 2645–2660
- Miller, B.P., Gallo, E., Wright, J.T., & Dupree, A.K., 2012, *ApJ*, 754, 2, id. 137
- Nymeyer, S., Harrington, J., Hardy, R.A., Stevenson, K.B., Campo, C.J., Madhusudhan, N., Collier-Cameron, A., Lored, Th., Bleicic, J., & Bowman, W.C., 2011, *ApJ*, 742, 1, id. 35
- Ordal, M.A., Bell, R.J., Alexander, R.W., Newquist, L.A., & Querry, M.R., 1988, *Applied Opt.*, 27, 1203

- Perryman, M.A.C., Lindegren, L., Kovalevsky, J., Hoeg, E., Bastian, U., Bernacca, P.L., Creze, M., Donati, F., Grenon, M., Grewing, M., van Leeuwen, F., van der Marel, H., Mignard, F., Murray, C.A., Le Poole, R.S., Schrijver, H., Turon, C., Arenou, F., Froeschle, M., & Petersen, C.S., 1997, *A&A*, 323, p.L49-L52
- Pillitteri, I., Wolk, S.J., & Sciortino, S., 2014, *A&A*, Vol.567, A128
- Press W.H., Teukolsky S.A., Vetterling W.T., & Flannery B.P., 1992, *Numerical Recipes in FORTRAN: The Art of Scientific Computing*, Cambridge University Press
- Roberge, A., Chen, C., Millan-Gabet, R., Weinberger, A.J., Hinz, Ph.M., Stapelfeldt, K.R., Absil, O., Kuchner, M., & Bryden, G., 2012, *PASP*, 124, 918
- Salz, M., Schneider, P.C., Czesla, S., & Schmitt, J.H.M.M., 2015, *A&A*, 576, A42
- Scott, A., & Duley, W.W., 1996, *ApJ Supplement*, 105, 401
- Seager S., Whitney B.A., & Sasselov D.D., 2000, *ApJ*, 540, 504
- Simmons, J.F.L. & Stewart, B.G., 1985, *A&A*, 142, 100
- Skrutskie, M.F., Cutri, R.M., Stiening, R., Weinberg, M.D., Schneider, S., Carpenter, J.M., & 25 other authors, 2006, *ApJ*, 131, 2, pp 1163-1183
- Southworth J., Hinse, T.C., Dominik, M., Glittrup, M., Jørgensen, U.G., Liebig, C., Mathiasen, M., Anderson, D.R., Bozza, V., Browne, P., et al, 2009, *ApJ*, 707, 1, pp. 167
- Spurr, R., 2006, *JQSRT*, 102, 316.
- Stam, D.M., Hovenier, J.W., & Waters, L.B.F.M., 2004, *A&A*, 428, 663672
- Torres G., Winn J.N., & Holman M.J., *ApJ*, 677, 1324-1342
- Torres, G., Fischer, D.A., Sozzetti, A., Buchave, L.A., Winn, J.N., Holman, M.J., & Carter, J.A., 2012, *ApJ*, 757, 161
- Von Zeipel, H., 1924, *MNRAS*, 84, p.665-683
- Walker, G.A.H., Croll, B., Matthews, J.M., Kuschnig, R., Huber, D., Weiss, W.W., Shkolnik, E., Rucinski, S.M., Guenther, D.B., Moat, A.F.J., & Sasselov, D., 2009, *A&A*, 482, 2, 691-697
- Wiktorowicz S.J., 2009, *ApJ*, 696, 1116
- Wiktorowicz S.J. & Matthews K., 2008, *PASP*, 120, 1282
- Wiktorowicz S. & Laughlin, G.P., 2014, *ApJ*, 795, 1, id 12
- Wiktorowicz S. & Nofi, L.A., 2015, *ApJ*, 800, L1
- Wiktorowicz S., Nofi L.A., Daniel J.-T., Kopparla P., Laughlin G.P., Hermis N., Yung Y.L., & Swain M.R., 2015, *ApJ*, 813, 48
- Wilkins, A., Delrex, L., Barker, A., Deming, D., Hamilton, D., Gillon, M., & Jehin, E., 2017, *ApJ Letters*, 836, 2, L24
- Wilson, R.E & Devinney, E.J., 1974, *ApJ*, 166, 605
- Wilson, R.E., 1979, *ApJ* 234, 1054
- Wright, E.L., Eisenhardt, P.R.M., Mainzer, A.K., Ressler, M.E., Cutri, R.M., Jarrett, Th., Kirkpatrick, J.D., Padgett, D. & 30 other authors, 2010, *ApJ*, 140, 6, pp 1868-1881
- Zahnle, K., Marley, M.S., Freedman, R.S., Lodders, K., & Fortney, J.J., 2009, *ApJ* 701, L20